CHINESE OPTICS LETTERS

Vol. 19, No. 8 | August 2021

Recent development of saturable absorbers for ultrafast lasers [Invited]

Mengyu Zhang (张梦羽), Hao Chen (陈 浩), Jinde Yin (尹金德), Jintao Wang (王金涛), Jinzhang Wang (王金章), and Peiguang Yan (闫培光)*

Shenzhen Key Laboratory of Laser Engineering, College of Physics and Optoelectronic Engineering, Shenzhen University, Shenzhen 518060, China

*Corresponding author: yanpg@szu.edu.cn

Received November 10, 2020 | Accepted March 3, 2021 | Posted Online August 5, 2021

As one of the greatest inventions in the 20th century, ultrafast lasers have offered new opportunities in the areas of basic scientific research and industrial manufacturing. Optical modulators are of great importance in ultrafast lasers, which directly affect the output laser performances. Over the past decades, significant efforts have been made in the development of compact, controllable, repeatable, as well as integratable optical modulators (i.e., saturable absorbers). In this paper, we review the fundamentals of the most widely studied saturable absorbers, including semiconductor saturable absorber mirrors and low-dimensional nanomaterials. Then, different fabrication technologies for saturable absorbers and their ultrafast laser applications in a wide wavelength range are illustrated. Furthermore, challenges and perspectives for the future development of saturable absorbers are discussed and presented. The development of ultrafast lasers together with the continuous exploration of reliable saturable absorbers will open up new directions for the mass production of the next-generation optoelectronic devices.

Keywords: SESAMs; low-dimensional materials; nonlinear optical properties; optical modulators; ultrafast lasers.
DOI: 10.3788/COL202119.081405

1. Introduction

The development of ultrafast laser technology has become one of the most cutting-edge domains and hot points in photonics and even modern science. Ultrafast laser technology is expected to make a breakthrough in numbers of fields and plays an important role in promoting the future development of science and technology. As one of the greatest inventions in the 20th century, the development of lasers has gone through nearly 60 years since the first, to the best of our knowledge, demonstration of coherent light generated from a flashlamp-pumped ruby crystal[1]. Many other types of lasers emerged soon after, including gas lasers[2], glass lasers[3], and semiconductor lasers[4]. It was not until the 1980s that stable passive mode-locking with a femtosecond (fs) pulse was demonstrated using a dye saturable absorber (SA) in a laser cavity[5]. In the early 1990s, Ti:sapphire mode-locked lasers with the Kerr-lens effect infinitely promoted the rapid development of fs laser technology, mainly manifesting in the huge reduction of pulse durations and the sharp increase of peak powers. The pulse durations have decreased from the original 100 fs to nearly sub-10-fs and even further narrowed to the astonishing magnitude of attosecond (10^{-18} s) via high-order harmonics[6–10]. Meanwhile, the peak power has been increased from megawatt (MW) to more than several petawatts (PW, $1\ \mathrm{PW} = 10^{15}$ W)[11,12]. Subsequently, a large range of revolutionary applications have been demonstrated to take full advantages of ultrafast lasers (e.g., fs spectroscopy, optical frequency comb, ultrafast and high-resolution imaging). These applications prove that fs laser technology is of great significance to fundamental scientific research[13–17]. Further, ultrafast laser technology has been widely used in industries, for example, lighting and displaying, remote sensing and environmental monitoring, biology and medical diagnosis, communication and national defense, and advanced manufacturing[17–20].

Mode-locking, which usually incorporates either active or passive pulse modulators, is a commonly used technique to generate ultrashort pulses. More specifically, active mode-locking requires an external signal normally driven by an acousto-optic or electro-optic modulator. A typical external sinusoidal signal periodically modulates the intracavity loss, the modulation rate of which is integer multiples of the cavity frequency[20]. A lithium-niobite-crystal-based electro-optic modulator can easily achieve several hundreds of gigahertz (GHz) repetition rate, which is desirable for high-capacity optical communication systems[21–25]. However, the pulse widths of actively mode-locked lasers are usually in the picosecond region. Passive mode-locking refers to the situations that ultrashort pulses are formed

through nonlinearities inside the cavity and can easily achieve fs pulses. For passive mode-locking, nonlinear optical modulators, named SAs, whose response to an entering optical pulse is intensity dependent, are used to obtain self-amplitude modulation. The earliest fs lasers based on SAs were realized in dye lasers for tens of fs pulses generation[26–28]. However, the dye lasers suffer from complex structure and poor environmental stability. In addition, the organic dyes are poisonous and require recycling, which limit their generalization. Then, self-mode-locking (i.e., Kerr-lens mode-locking), generated from the third-order nonlinearity of the gain medium, emerges as another new mode-locking mechanism for fs pulses generation[29–31]. Although Kerr-lens mode-locking does not require a complex modulator, it depends on external disturbance for self-starting and is extremely sensitive to misalignment. The development of semiconductor epitaxy technology and semiconductor bandgap engineering makes semiconductor SA mirrors (SESAMs) the hottest candidates for passive mode-locking[32]. The precisely controllable fabrication of SAs is a huge leap forward in passively mode-locked lasers. Nowadays, SESAMs have been commonly adopted in commercial mode-locked laser systems due to their validity and reliability at specific wavelengths. Nevertheless, the fabrication of SESAMs requires complex procedures as well as expensive equipment. In addition, SESAMs are bulky and inflexible, and need spatial alignment, which is inconvenient for fiber laser systems. The limitations of SESAMs have triggered the development of novel low-dimensional materials (LDMs) SAs, which can be easily integrated into various configurations. As strong contenders for SESAMs, LDMs have already been widely applied in ultrafast laser systems[33–38].

Here, we review the recently studied advances of SAs in terms of fabrication and applications. In Section 2, we mainly introduced the fundamental properties of the most widely studied semiconductor materials including SESAMs, carbon nanotubes (CNTs) and graphene, and transition metal dichalcogenides (TMDCs). This was then followed by the fabrication of the SAs and their ultrafast laser applications both in free-space and fiber laser systems. In the last section, we discussed the pros and cons of the present SA fabrication methods and ended up with perspectives on LDMs-based SAs.

2. Fundamental of Properties of Saturable Absorbers

Saturable absorption properties are of great significance for passively mode-locked lasers. Pulse operation initiates from the random noise sequence in the laser cavity. When an optical pulse propagates through the SA, its wings experience more loss than the central part, because high intensity more easily saturates the absorber. As a result, the loss modulation is synchronized automatically with the laser pulses. The Pauli blocking effect can explain the saturable absorption phenomenon at the microlevel. When high-intensity light interacts with a nonlinear optical material, electrons in the valence band absorb the incident photons and transit to a higher conduction band. For low-incident intensity, most of the photons are absorbed, hence, resulting in low transmission. Under high incident beam intensity, the conduction band is full with electrons and cannot accept more electrons due to the Pauli blocking effect. Consequently, most of the photons transit through the material resulting in high transmission. The basic mechanism for mode-locking can be easily understood by considering the SA as a passive optical modulator whose absorption (loss) is intensity-dependent, which can be described by a two-level model:

$$\alpha(I) = \frac{\alpha_{\text{sat}}}{1 + I/I_{\text{sat}}} + \alpha_{\text{non-sat}}, \tag{1}$$

where α_{sat} is the modulation depth (saturable loss), $\alpha_{\text{non-sat}}$ is non-saturable loss, and I_{sat} is the saturation intensity (required intensity to reduce the absorption by $0.5\alpha_{\text{sat}}$). In this section, we mainly focus on the fundamental properties of the most concerned SAs (SESAMs and LDMs), especially their nonlinear optical properties.

2.1. SESAMs

Since 1990, Keller *et al.* have attempted to implement semiconductor SAs into lasers for self-starting mode-locking[39]. Experimental reports have demonstrated that stable mode-locking can be obtained by deliberately designing macroscope parameters of SESAMs (such as carrier lifetime, saturation energy, and modulation depth)[21]. Dynamics of the SESAM are complex, in that the pulse evolution must be treated with a modified Ginzburg–Landau equation with several nonlinear non-conservative terms[22]. The saturable loss of a SESAM is given by

$$\frac{\partial \delta_s(t)}{\partial t} = -\frac{\delta_s(t) - \Delta R}{\tau_{\text{rec}}} - \frac{|\varphi(t)|^2}{E_{\text{sat}}}\delta_s, \tag{2}$$

where ΔR is the saturable loss of an unexcited absorber (modulation depth), $|\varphi(t)|^2$ is the optical field intensity, τ_{rec} is the absorption recovery time, and E_{sat} is the absorber saturation fluence. The solution of Eq. (2) is

$$\delta_s(t) = \frac{\Delta R}{f(t)}\left[\frac{1}{\tau_{\text{rec}}}\int f(t)\mathrm{d}t + 1\right], \tag{3}$$

where

$$f(t) = \exp\left\{\int\left[\frac{1}{\tau_{\text{rec}}} + \frac{|\varphi(t)|^2}{E_{\text{sat}}}\right]\mathrm{d}t\right\}. \tag{4}$$

For practical purposes, we assume that $\tau_{\text{pulse}} \ll \tau_{\text{rec}}$, where τ_{pulse} is the pulse duration and the incident pulse energy E_p is proportional to $\int_{-\infty}^{\infty}|\varphi(t)|^2\mathrm{d}t$. Therefore, $\delta_s \approx \Delta R e^{-E_p/E_{\text{sat}}}$, and the effective average loss for this pulse can be simplified as $\delta_p = \Delta R(1 - e^{-E_p/E_{\text{sat}}})(E_p/E_{\text{sat}})$. The mirror reflectivity is $R = 1 - \delta_p - \alpha_0$, where α_0 is non-saturable loss. SAs can be divided into slow and fast ones. Most of the real SAs are slow ones with recovery time at the nanosecond regime, while the fast SA (like Kerr lens) has a recovery time as fast as the fs regime. A previous

report has shown that a slow SA can generate pulses much shorter than the recovery time of the absorber[40]. However, the fast SA is more stable against multi-pulse in a high-power laser cavity[41]. Reference [42] provides a comprehensive discussion on the relationship between pulse duration and recovery time based on analytical and numerical calculation methods.

Besides, saturation fluence plays an important role in the reduction of the mode-locking threshold and the avoidance of optical damage. The saturation energy of commercial SESAMs is typically centered between 50 and 100 $\mu J/cm^2$. Keller *et al.* have presented two novel SESAM designs to decrease the saturation energy[43]. Low saturation energy is also suitable for ultrahigh repetition rate (i.e., $\gg$ 1 GHz) operation[43]. In addition, a multi-layer quantum well (QW) can be chosen to obtain a large modulation depth, whereas the modulation depth should not be too high to avoid the *Q*-switching operation[44]. Moreover, several approaches have been adapted to improve the damage threshold, such as careful design of an anti-resonant cavity, expanding the input spot size, coating a protecting dielectric film on the surface of the SESAMs, or adopting quantum dots (QDs) SESAMs[41,45,46].

2.2. Low-dimensional materials

2.2.1. CNTs and graphene

The unique lattice structure of carbon-based LDMs (i.e., CNTs, graphene) endows them with superior linear and nonlinear optical properties. The explosion in research of CNTs was initiated by the group of Iijima in 1991[47]. The angle that the sheet rolls to form a tube determines the electronic properties of the CNTs, and the band energy of the CNTs is inversely proportional to the diameter[48,49]. Experiments have demonstrated that CNTs with semiconducting behavior own an ultrafast recovery time (~30 ps)[50], whereas in practice situations, nanotubes containing metallic and semiconducting behavior are entangled with each other, resulting in a recovery time of less than 1 ps[51]. The distribution of diameters so far can be reduced to a desired range by precise control of the growth conditions. Additionally, the one-dimensional (1D) nature of the material gives rise to Van Hove singularities with a low density of states resulting in a small saturation fluence[49]. CNTs-SA mode-locking in an erbium (Er)-doped fiber laser (EDFL) was firstly, to the best of our knowledge, reported by Set *et al.* in 2004[52]. The as-prepared CNT films can be applied for wideband mode-locking with absorption wavelengths ranging from the visible to mid-infrared (MIR)[53–56].

Graphene is a semimetal with a honeycomb lattice structure. The linear absorption of single-layer graphene is determined by the fine structure constant (≈2.29%), which is independent of the frequency of the incident light[57]. Nonlinear absorption can be obtained under stronger illumination that the modulation depth of graphene scales up with the number of layers[58,59]. However, the observed modulation depth reduced with the layer number further increasing. This can be explained as follows: not all of the graphene sheets are saturated, and the SA cannot be fully bleached. Therefore, it is necessary to adopt the appropriate layer number of SAs in practical applications. In addition, the linear dispersion of Dirac electrons makes graphene an effective SA for ultrafast pulses generation, where the fast relaxation time (corresponding to carrier-carrier intraband scattering rates) is in the fs scale as well as the slow relaxation time (correlating with electron-hole interband recombination) in the picosecond scale[60,61]. In 2009, Bao *et al.* firstly, to the best of our knowledge, reported graphene-SAs for ultrafast lasers[62]. Compared with SESAMs or CNT-SAs, the most distinctive performance of graphene is the extremely broad absorption bandwidth covering from the ultraviolet to microwave[63]. Thus far, graphene-based SAs have been used for 0.8 to 2.9 μm mode-locked lasers[64–68].

2.2.2. TMDCs

Similar with graphene, bulk TMDCs are formed by stacking single-material layers with weak van der Waals forces. TMDCs exhibit rich physical behaviors from wideband insulators to narrowband semiconductors, semimetals, or metals, which offer evident optical responses over an extremely wide spectral range (from ultraviolet to terahertz or even microwave)[69,70]. One of the most remarkable properties of TMDCs is that they exhibit an indirect to direct bandgap transition when decreasing the layer number. For example, the indirect bandgap of bulk MoS_2 is 1.29 eV and changes to a direct bandgap (1.9 eV) when decreasing to a monolayer[71]. Similar to MoS_2, WS_2 and $MoSe_2$ also experience the transition from an indirect bandgap of 1.3 eV (1.1 eV) to a direct bandgap of 2.1 eV (1.55 eV)[72,73]. The optical absorbance of monolayer TMDCs at their resonance wavelength is extremely large, which can reach 10% compared with that of monolayer graphene (2.3%). The strong light–matter interaction in TMDCs makes it possible for the generation of high-order susceptibility, which offers a wide platform for ultrafast photonics. Another unique property of TMDCs is the emergence of strong excitonic effects, which can absorb photon energies less than the bandgap. Photons with sub-bandgap energies can saturate the material due to Pauli blocking, enabling mode-locking at the near-infrared (NIR) wavelength[70].

3. Fabrication and Ultrafast Laser Applications of SAs

3.1. SESAMs mode-locked lasers

The emergence of SESAMs is considered the revolutionary improvement for ultrafast lasers. Molecular beam epitaxy (MBE) and metal-organic vapor phase epitaxy (MOVPE) are two generally used fabrication techniques with different growth pressures and temperatures. A SESAM typically consists of a high-quality distributed Bragg reflector (DBR) followed by a multi-QWs or QDs absorption layer. The design of the DBR and absorption region has been optimized for desirable optical parameters, such as the modulation depth, saturation energy, non-saturable losses, and recovery time[74–77]. To date, most SESAMs are based on QW absorbers. Nevertheless,

QD-SESAMs show great degrees of design freedom in the control of saturable parameters[78]. The additional parameter of the dot density combined with the field enhancement makes it possible for independent control of saturation energy and modulation depth[75]. Furthermore, the absorption wavelength can be adjusted with different QD sizes. High-temperature grown InAs QD-SESAMs working at 1.55 μm were shown in 2019[79]. Keller *et al.* have demonstrated SESAM mode-locked vertical external-cavity surface-emitting lasers (VECSELs) based on QDs gain material and pushed the laser performance to a new level. In 2020, the first anti-resonant QD-SESAMs with high-temperature stability (withstand the long DBR overgrowth at 600°C) were demonstrated, which provides great opportunities for the monolithic integration into external-cavity surface-emitting laser (MIXSEL) devices[80]. Latterly, Ko *et al.* have investigated the operating characteristics of the pulses with different SESAM positions. The results can give some good ideas to those who are interested in the improvement of the SESAMs-assisted mode-locked lasers[81].

After nearly a decade of efforts, SESAM mode-locking has motivated the frontier in hundred GHz repetition rates (up to more than 160 GHz at 1 μm and 100 GHz at 1.5 μm)[82,83]. Furthermore, SESAM mode-locked thin-disk lasers (TDLs) have pushed the pulse energies up to more than 80 μJ at a megahertz (MHz) repetition rate without additional amplification, and the average output power has been scaled to 350 W with 39 μJ pulse energies based on the $Yb:Y_3Al_5O_{12}$ (Yb:YAG) (~1 μm), $Tm:Ca_3Li_xNb_{1.5x}Ga_{3.5-2x}O_{12}$ (Tm:CLNGG) (~2 μm) thin-disk gain material (Fig. 1)[84,85]. Figure 1(a) demonstrates the schematic of the mode-locked Yb:YAG TDL cavity. Figures 1(b) and 1(c) are beam profiles at 350 W output power in continuous wave (CW) and mode-locked operation.

SESAM mode-locked solid-state lasers have stimulated the novel ultrafast semiconductor disk laser (SDL), which bridges the gap between the solid-state laser and the solid-state TDL. VECSELs combining the advantage of semiconductor gain materials and SESAMs possess large gain cross section and are therefore ideally suited for high repetition rates, high average output powers generation. Additionally, advantages such as mass production on the wafer scale and easy integration into complex optical circuits are important for practical applications[86,87]. After the first, to the best of our knowledge, demonstration of a passively mode-locked VECSEL in 2000, high repetition rates in the multi-GHz range and pulse widths reaching the fs level are no longer an issue[88]. The large emitting area of the VECSEL allowed the average output power up to 5.1 W and the fundamental repetition rate scaled up to 50 GHz with the peak power over 4.3 kW[89–93]. Figures 2(c) and 2(d) display the measured laser performance with different cavity lengths and output couplers. The shortest pulse of 196 fs was obtained with a 1.67 GHz repetition rate and a 112 mW output power[89]. Then, a sub-100-fs (95 fs) pulse directly from a mode-locked VECSEL without compression has also been reported at a 1025 nm central wavelength[90].

Many applications require more compact and simpler fs sources with a minimum number of components. A logical following step toward more compact SDL is the MIXSEL, which integrates both the gain and the absorber within one wafer to improve the integration level so that stable self-starting mode-locking can be achieved in a simple straight cavity. After the first, to the best of our knowledge, demonstration of optically pumped MIXSEL in 2007[94], the MIXSEL cavity enabled repetition rate scaling up to 101.2 GHz[95]. With the progress in QD SESAMs, the MIXSEL allowed the average output power to

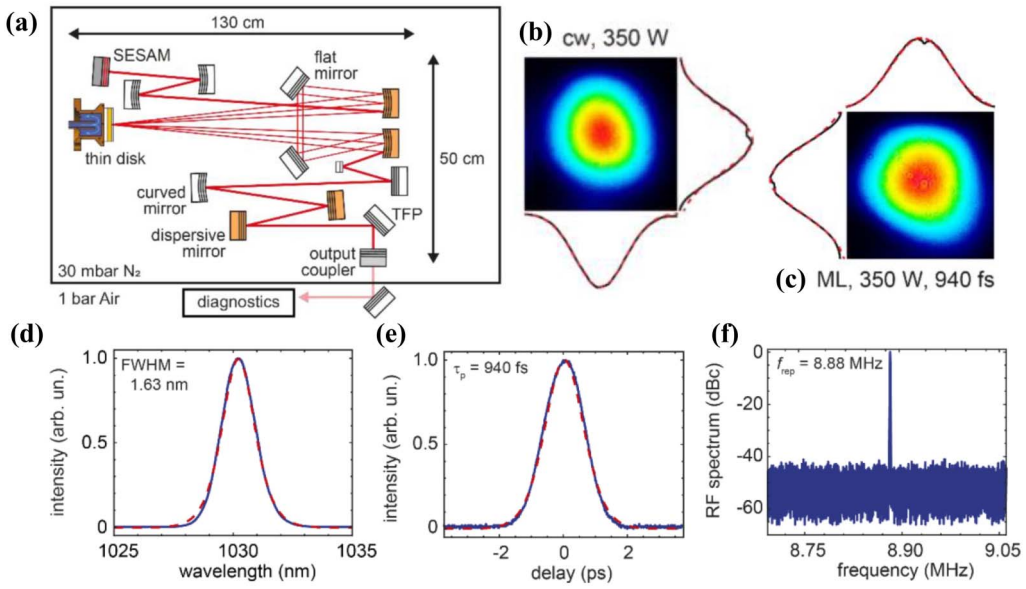

Fig. 1. SESAM-based mode-locked Yb:YAG TDL. (a) Schematic of the cavity design. (b) Beam profile at 350 W output power in CW operation. (c) Beam profile at 350 W in mode-locked operation. The vertical and lateral cuts of the beam are depicted as red lines with Gaussian fits. (d) Optical spectrum with the central wavelength of 1030 nm. (e) Autocorrelation (AC) trace. (f) Radio frequency (RF) spectrum with 42 dB signal-to-noise ratio. (a)–(f) Reproduced with permission[85]. Copyright 2019, Optical Society of America.

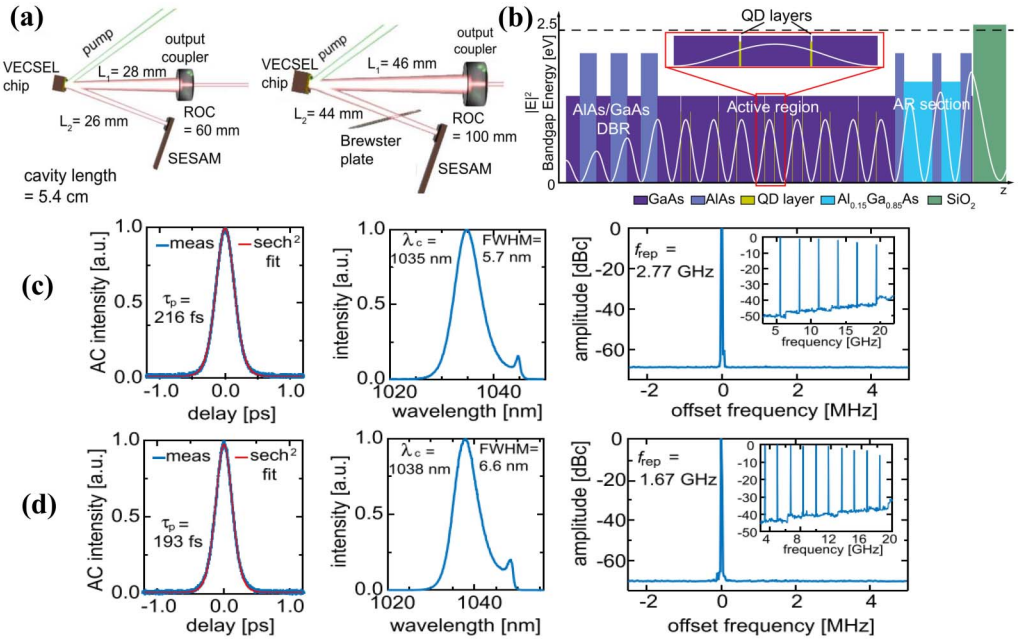

Fig. 2. Quantum dots (QDs) as active media for ultrafast mode-locked VECSEL. (a) V-shaped cavity designed with the SESAM and output coupler as end mirrors and the VECSEL gain chip as the folding mirror. (b) Epitaxial structure of the QD VECSEL and the standing wave intensity profile at the central wavelength of 1035 nm. (c) and (d) SESAM mode-locked VECSEL results with different cavity designs. (c) Pulse characterizations are measured with a pulse duration of 216 fs and a full width at half-maximum (FWHM) of 5.7 nm at 2.77 GHz repetition rate. (d) Pulses of 193 fs with 6.6 nm FWHM bandwidth and 1.67 GHz repetition rate. Reproduced with permission[89]. Copyright 2018, IEEE.

increase to 6.4 W[96]. The schematic design and scanning electron microscope (SEM) image of the MIXSEL layer stack are given in Figs. 3(a) and 3(b). The straight laser cavity with only two components has generated 28 ps pulses with 2.5 GHz repetition rate at 959 nm central wavelength [Figs. 3(b)–3(e)]. Lately, a new record was obtained by optimizing the gain structure and thermal management, where the MIXSEL achieved a pulse duration of 144 fs at a center wavelength of 1033 nm with a pulse repetition rate of 2.73 GHz[97]. Though VECSEL and MIXSEL are not expected to provide higher average output powers than mode-locked solid-state TDLs or shorter pulses than mode-locked Ti:sapphire lasers, they do provide simple solutions for compact, low-cost ultrafast lasers in the multi-GHz repetition rate region.

The wavelength flexibility and controllable fabrication make SESAMs superior to other types of SAs. However, limited by the available gain materials and saturable absorption materials, SESAMs mode-locking in the MIR or extreme ultraviolet (XUV) have not reached the same mature degree as in the NIR. In 2017, Labaye *et al.* reported the first intracavity high-harmonic generation (HHG) inside a TDL oscillator for XUV light generation[98]. An illustration of the experimental setup is shown in Fig. 4. The mode-locked system was based on a diode-pumped $Yb:Lu_2O_3$ thin disk and a SESAM. When the high-pressure gas jet was emitted into the beam focus, high harmonics of orders up to the 17th (60.8 nm) were detected with 255 fs pulse width, 64 MW intracavity peak power, and 17.35 MHz repetition rate. Due to the relatively long recovery times and the poor saturable absorption properties of GaAs-based SESAMs, GaSb-based SESAMs exhibiting better lattice matching, lower non-saturable loss, and significantly shorter recovery time after appropriate post-processing technology, have been explored for MIR region mode-locking. They have been successfully adopted both in solid-state lasers and SDLs for sub-picosecond pulses generation[99–103]. Zhao *et al.* reported the first, to the best of our knowledge, sub-100-fs mode-locked Tm/Ho:$CaYAlO_4$ laser employing a GaSb-SESAM[103]. As shown in Fig. 5, pulses as short as 87 fs are produced at a 2042 nm wavelength with an 80.45 MHz repetition rate. Nevertheless, mode-locking operation beyond 3 μm is hampered due to the limited absorption wavelength of GaSb-SESAMs.

More details are listed in Table 1, which collects some typical laser performances of SESAM mode-locking from visible to MIR wavelengths.

3.2. LDMs-based mode-locked lasers

3.2.1. LDMs-SAs for solid-state lasers

The fabrication of LDMs-based SAs is usually directly depositing or transferring nanomaterials onto optical substrates to form reflection or transmission type structures. It is worth noting that the insertion loss should be well designed due to a much lower single-pass gain in solid-state lasers. Passively mode-locked all-solid-state lasers based on CNT-SAs have been successfully investigated from 0.8 to 2.1 μm wavelengths[121–126]. The single-walled carbon nanotube SA mirror (SWCNT-SAM) mode-locking was firstly, to the best of our knowledge,

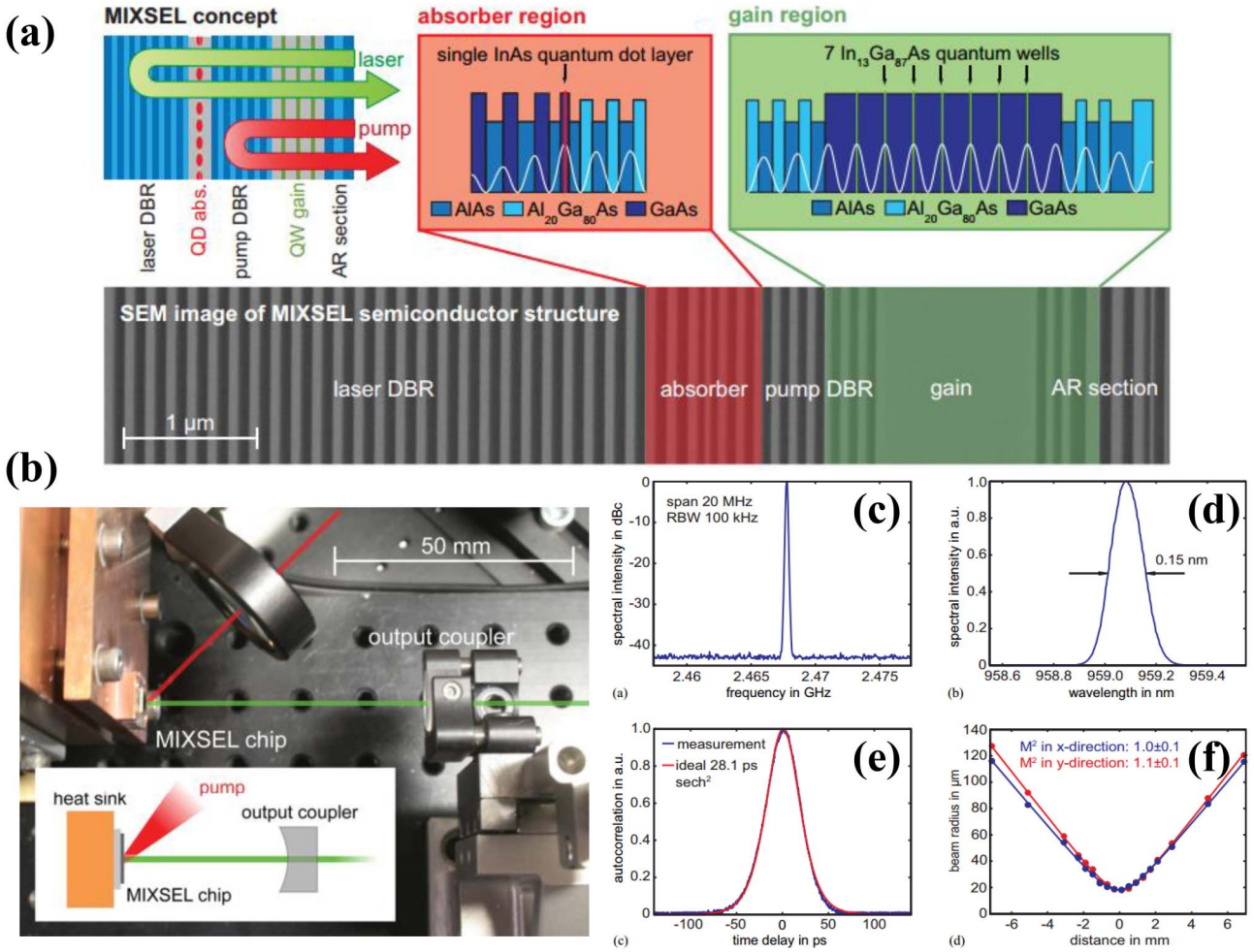

Fig. 3. Optically pumped high-power MIXSEL. (a) MIXSEL concept and SEM image: the MIXSEL semiconductor consists of two highly distributed Bragg reflectors (DBRs), a QD saturable absorption layer, a quantum well (QW) gain section, and an anti-reflective (AR) coating. (b) Photograph and sketch of the MIXSEL cavity: the sample straight cavity is formed by a MIXSEL chip and an output coupler. (c) RF spectrum, (d) optical spectrum, (e) AC trace intensity, and (f) beam quality measurement. (a)–(f) Reproduced with permission[96]. Copyright 2010, Optical Society of America.

demonstrated with the gain medium of Er/Yb co-doped glass in 2005[121]. Since then, pulse durations from picoseconds to fs have been achieved in various CNTs mode-locked lasers including Ti:sapphire (~800 nm)[122,123], Yb:$KLu(WO_4)_2$ (Yb:KLuW), Yb:YAG (~1 μm)[124,125], Cr:forsterite (~1.25 μm)[126], Tm:$Ca_3Na_xNb_{1.6875}Ga_{3.1875}O_{12}$ (Tm:CNNGG), Cr:ZnS (~2 μm, 2.4 μm)[127,128]. The fast and slow recovery times of SWCNT-SAs are 0.25 ps and 1.16 ps, which are comparable to GaAs-based SESAMs[129]. However, the diameters and chirality of the SWCNTs cannot support operation beyond 2100 nm due to the difficulty insynthesis. Later, other LDMs-based SAs such as graphene have also been successfully employed in all-solid-state lasers for ultrashort pulses generation. Ma *et al.* reported the first, to the best of our knowledge, ultra-broadband graphene-gold film SA mirror (GG-SAM) mode-locking in Yb:$YCa_4O(BO_3)_4$ (Yb:YCOB) (~1 μm), Tm:$Ca_3Li_xNb_{1.5x}Ga_{3.5-2x}O_{12}$ (Tm:CLNGG) (~2 μm), and Cr:ZnSe (~2.4 μm) bulk lasers with the operation range exceeding 1300 nm (from 2310 nm to 2426 nm)[130]. Similarly, graphene mode-locking was also achieved in Nd:$Y_3Al_5O_{12}$ (Nd:YAG) crystal lasers, realizing an ultra-high repetition rate of 11.5 GHz at 1064 nm[131]. Remarkably, with graphene-SAs, the generation of sub-100-fs (41 fs) pulses around 2.4 μm was achieved in a Cr:ZnS laser[132]. Apart from CNTs and graphene, other novel LDMs-based SAs have also been proved to support solid-state mode-locking, which generally operates around 1–2 μm.[133,134] Recently, optically pumped SDLs mode-locked by CNTs and graphene-SAs have also been reported. Seger *et al.* reported the CNT mode-locked SDL for the first time, to the best of our knowledge[135]. Stable mode-locking was obtained with 1.23 ps pulse width and 613 MHz repetition rate. Zaugg *et al.* demonstrated tunable VECSEL mode-locking with different gain chips by employing a single-layer graphene-SAM (G-SAM)[136]. The laser cavity is sketched in Fig. 6(a), and the picture of 8/λ G-SAM is displayed in Fig. 6(b). The maximum tuning range (from 935 nm to 981 nm) is achieved with a QW VECSEL, which is larger than that of previously reported SESAM mode-locked VECSELs [Fig. 6(e)]. The mode-locked

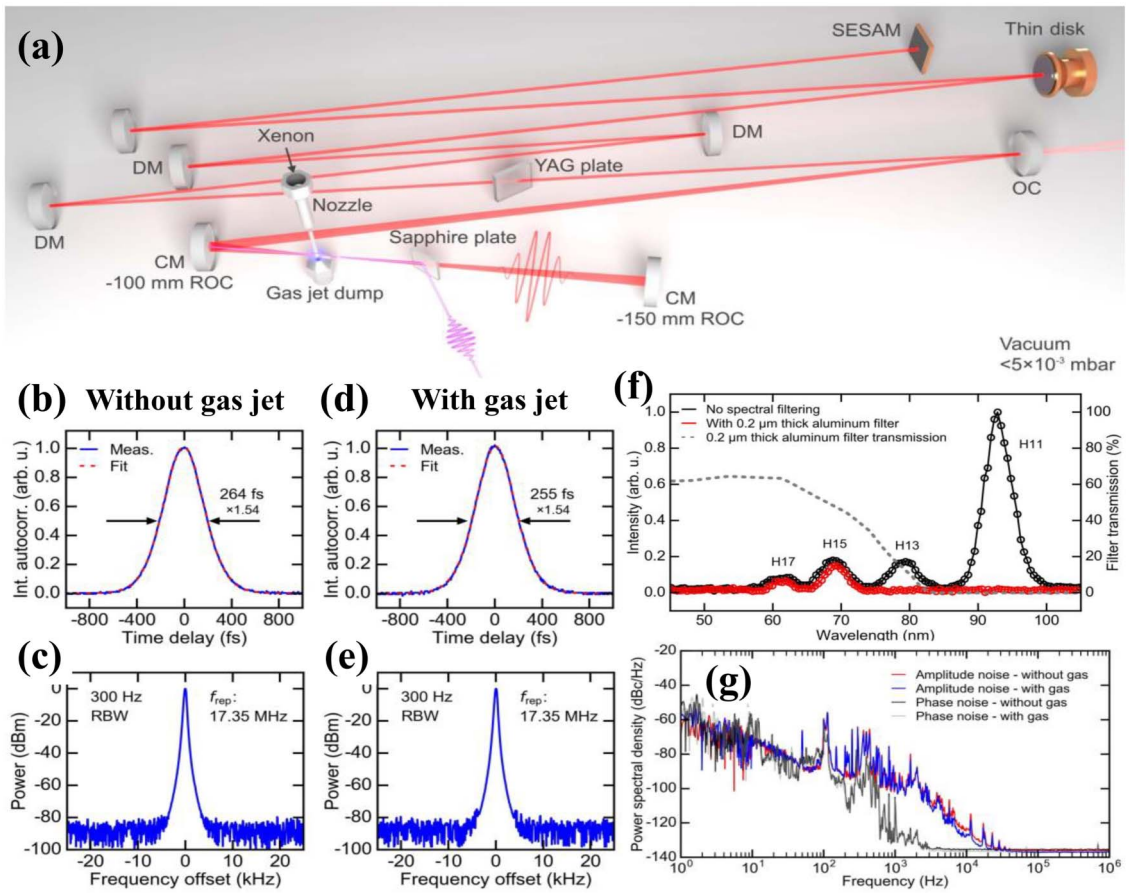

Fig. 4. XUV light source generation based on HHG inside a mode-locked TDL. (a) Illustration of the experimental setup. (b) AC trace and (c) RF spectrum without a high-pressure xenon gas jet. (d) AC trace and (e) RF spectrum with high-pressure xenon gas jet. (f) Optical spectrum of the generated XUV light. (g) Amplitude and phase noise measurements of the mode-locked TDL with and without gas. (a)–(g) Reproduced with permission[98]. Copyright 2017, Optical Society of America.

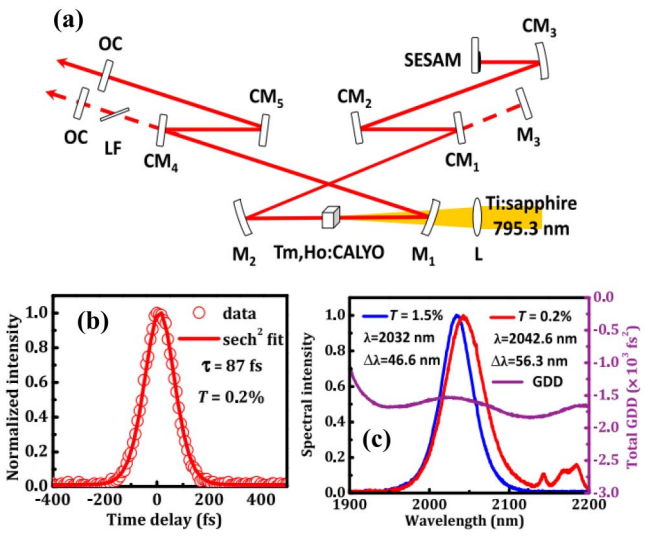

Fig. 5. SESAM mode-locked Tm,Ho:$CaYAlO_4$ laser. (a) Schematic of the mode-locked Tm,Ho:$CaYAlO_4$ laser cavity. (b) AC trace of the mode-locked Tm,Ho:$CaYAlO_4$ laser and (c) the corresponding optical spectra. (a)–(c) Reproduced with permission[103]. Copyright 2018, Optical Society of America.

VECSEL delivered the repetition rate up to 2.48 GHz with the pulse duration minimizing to 466 fs [Figs. 6(c) and 6(d)]. In particular, Husaini *et al.* reported a mode-locked VECSEL with 10 W output power and 353 fs pulse duration using a graphene mirror[137].

More details are listed in Table 2, which collects some typical laser performances of LDMs mode-locking in solid-state lasers.

3.2.2. LDMs-SAs for fiber lasers

Recently, the study on fiber lasers has shown explosive growth owing to their inherent advantages in the respect of flexibility, high beam quality, alignment-free format, and favorable heat sinking. LDMs can be easily integrated into various optical configurations to achieve alignment-free and all-fiber formats, which cannot be realized for SESAMs.

A. LPE technique and ink-jet printing method

The solution-processing technique is widely used for high-yield few-layer nanosheets preparation, which includes either chemical exfoliation (e.g., lithium ion intercalation) or liquid phase exfoliation (LPE)[139,140]. The as-prepared nanosheets can then be incorporated with fiber configurations via series

Table 1. Passively Mode-Locked Solid-State Lasers Based on SESAMs..

Gain materials	Modulation depth (%)	τ_p (fs)[a]	λ (nm)[b]	f_{rep} (MHz)[c]	P_{out} (mW)[d]	Slope efficiency (%)	Pump source[e]	Ref.
Pr^{3+}:$LiYF_4$	\	\	523	\	2900	79	497 DL	[104]
Ti:sapphire	\	68	816	379	200	10	InGaN DL	[105]
Yb:CNGG	0.9	55	1051.5	87	60	1	DBR DL	[106]
Yb,Na:CNGG	0.6	45	1061	104	734	68.5	980 DL	[107]
Yb:$CaGdAlO_4$	\	166	1050	10.6	1200	2.8	980 DL	[108]
Yb:KGW	0.5	56	1040	77.3	1950	\	980 DL	[109]
Er:Yb:glass	0.4	4700	1535	9788	9	\	980 DL	[110]
Er:Yb:glass	\	5400	1544.4	6803.3	30	\	980 DL	[111]
Tm,Ho:$CaYAlO_4$	\	87	2042.6	80.45	27	22	TSL	[103]
Tm:$LuScO_3$	1	170	1973–2142	115.2	190	33	TSL	[112]
Cr:ZnSe	\	408	2042	127	403	12.2	TDFL	[113]
Tm:$(Lu_{2/3}Sc_{1/3})_2O_3$ ceramic	\	74	2057	78.9	175	34	TSL	[114]
Tm,Ho:CNGG	\	73	2061	89.3	36	\	TSL	[115]
Cr:ZnSe	\	100	2450	215	100	\	EDFL	[116]
Cr:ZnS	\	130	2375	180	130	\	EDFL	[117]
Yb:Lu_2O_3 disk	1.1	616	1033	10	82,000	44	DL	[118]
Yb:YAG disk	2.7	780	1030	10.96	210,000	\	940 DL	[119]
Yb:YAG disk	1.1	940	1030	8.88	350,000	\	DL	[85]
Yb:Lu_2O_3 disk	1.6	255	60.8	17.35	320,000	\	976 DL	[98]
VECSEL	1.4	216	1035	2770	269	2.1	DL	[89]
VECSEL	\	95	1025	2200	90	\	790 DL	[90]
VECSEL	0.5	682	1030	1710	5100	\	808 DL	[91]
VECSEL	\	400	1013	1670	3300	2.9	808 DL	[93]
VECSEL	2	5000	1341	1030	1670	\	980 DL	[120]
MIXSEL	\	570	964	101.2	127	\	808 DL	[95]
MIXSEL	\	28,100	959	2470	6400	17.3	808 DL	[96]
MIXSEL	\	144	1033	2730	30	<0.5	808 DL	[97]

[a] τ_p, pulse width.

[b] λ, central wavelength.

[c] f_{rep}, repetition rate.

[d] P_{out}, output power.

[e] DL, diode laser; TSL, Ti:sapphire laser; EDFL, erbium-doped fiber laser; TDFL, thulium-doped fiber laser.

methods (e.g., optical adsorption, spin-coating, drop-coating, vacuum filtration, or mixing with polymer)[141–144]. A commonly used SA fabrication method is incorporating nanosheets with polyvinyl alcohol (PVA) solutions and naturally drying to form freestanding polymer composites[139]. For example, CNT-PVA has been used in Yb-, Er-, and Tm-doped fiber lasers (TDFLs) for fs pulses generation[145–147]. Figure 7(a) displays the SWCNT-PVA mode-locked fiber laser, and stable sub-100-fs pulses (~74 fs) were achieved by the all-fiber stretched pulse design[145]. As is shown in Fig. 7(c), the spectral width was

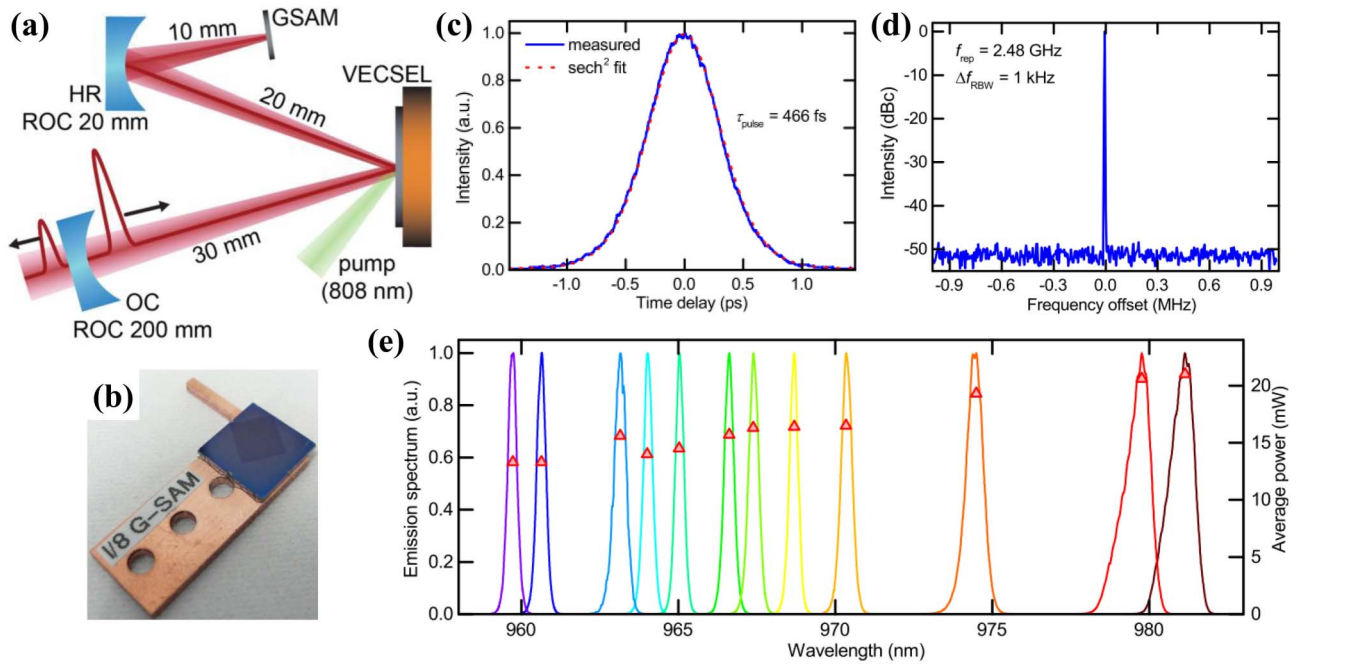

Fig. 6. (a) Schematic of the mode-locked VECSEL cavity. OC, optical coupler mirror; HR, highly reflective folding mirror; GSAM, graphene SAM. (b) Picture of the GSAM by transferring single-layer graphene on an 8/λ SiO_2. (c) AC trace and (d) RF spectrum centered at the repetition rate of 2.5 GHz with 1 kHz resolution. (e) Tunable optical wavelength (from 935 to 981 nm) and average output powers with different gain chips. (a)–(e) Reproduced with permission[136]. Copyright 2013, Optical Society of America.

measured to be 63 nm. However, the poor thermal damage threshold of the polymer limits their applications for high energy lasers. In 2007, Nicholson *et al.* proposed the optically driven deposition method for the fabrication of SWCNT-SAs[148]. The deposition process arises from the gradient force of light and thermophoresis of nanomaterials. By applying SWCNTs-SAs into an Yb-doped and Er-doped laser, stable mode-locking could be obtained with pulse durations of 137 fs and 247.5 fs, respectively. Furthermore, Sobon *et al.* have fabricated CNT films with thickness ranging from 50 to 200 nm via a vacuum filtration technique[149]. The shortest pulse duration was achieved by using a 100-nm-thick SWCNT layer, generating the bandwidth and pulse duration of 8.5 nm and 501 fs, respectively. Recently, Liu *et al.* fabricated an $AuTe_2Se_{4/3}$–SA by directly dripping the dispersion on the fiber end-face. Applying the $AuTe_2Se_{4/3}$–SA into an EDFL, ultrashort pulses (147.7 fs) operating at 1557.53 nm were realized with high stability (91 dB SNR)[150].

Although excellent laser output performances have been obtained with fiber-end-face-integrated SAs, the mode-locking stability gradually deteriorates by increasing the pump power. Therefore, tapered-fiber (TF) and side-polished fiber (SPF)-based SA structures are proposed, in which the light–matter interaction is processed via the evanescent wave. The first, to the best of our knowledge, TF-integrated CNT mode-locked laser was reported in 2007, which delivered 694 fs/1.7 nJ pulses with a fundamental repetition rate at 13.3 MHz[151]. Since then, numerous nanomaterials incorporated with TF/SPF have been reported for broadband mode-locked fiber lasers[152–156]. For LDMs deposition, a frequently used method is fixing the TF in a groove and adsorbing the nanomaterials via the capillary effect or optical gradient force. However, it is challenging to exactly control the deposition area with high continuity. We have built a photonic crystal fiber (PCF)-assisted deposition system where the PCF sprinkler is controlled by a three-dimensional (3D) adjusting mount [Fig. 8(a)][155]. By applying the HfS_2–SA into an EDFL, soliton mode-locking centered at 1562 nm was achieved with 221.7 fs ultrashort pulses. Figure 8(f) records the optical spectra of the soliton mode-locking operation for 4 h, which suggests the high stability of the laser cavity. Furthermore, ReS_2 films with different thicknesses were fabricated by the vacuum filtration method to form a double-covered ReS_2 microfiber (DCRM) SA[157]. The nonlinear transmittance of the ReS_2 SA at 1550 nm is shown in Fig. 9(c) with the modulation depth of 0.25%. Mode-locking operation was observed at the 1563 nm wavelength with a pulse duration of 3.8 ps. The main advantages of this type of SA devices are ease of fabrication and resistance to optical damage.

Although the LPE technique greatly facilitates the investigations on two-dimensional (2D) materials, the SA devices resulting from it suffer from the limitations of repeatability and durability. Inkjet printing provides a scalable craftsmanship that enables mask-less patterning with high resolution on flexible substrates. Indeed, 2D materials such as graphene, MoS_2, black phosphorus (BP), and MXenes have already been introduced to inkjet printing systems[158–160]. There are several challenges

Table 2. Passively Mode-locked Solid-state Lasers Based on LDM-SAs.

Gain materials	Nanomaterials	Modulation depth (%)	τ_p (ps)[a]	λ (nm)[b]	f_{rep} (MHz)[c]	P_{out} (mW)[d]	Pump source[e]	Ref.
Ti:sapphire	SWCNT	\	0.2	810	110	45	AL	[121]
Ti:sapphire	SWCNT	0.15	0.062	800	99.4	600	532 nm DL	[122]
Yb:KLuW	SWCNT	0.25	0.115	1045	89	53	TSL	[123]
Yb:KYW/KYW	SWCNT	0.21	0.083	1038	84	24	TSL	[124]
Yb:YAG	SWCNT	\	2	1030.3	2080	322	DL	[125]
Cr:forsterite	SWCNT	0.4	0.12	1250	79.1	202	YFL	[126]
Tm:CNNGG	SWCNT	0.5	0.084	2018	89.9	22	TSL	[127]
Cr:ZnS	CNT	\	0.061	2350	250	950	EDFL	[128]
Tm:KY$(WO_4)_2$	PbS QD	\	\	1936	185	20	802 DL	[138]
Yb:YOCB	Graphene	\	0.152	1037	99.9	53	980 DL	[130]
Tm:CLNGG	Graphene	\	0.354	2010	98	97	790 DL	[130]
Cr:ZnSe	Graphene	\	0.116	2352	99	66	EYFL	[130]
Nd:YAG	Graphene	\	16	1064	11,500	12	809 DL	[131]
CrZnS	Graphene	\	0.041	2370	108	250	EDFL	[132]
Nd:YVO_4	MoS_2	7	12.7	1064.2	88.3	89	808 DL	[133]
Nd:$LuVO_4$	$PtSe_2$	12.6	15.8	1066.573	61.3	180	808 DL	[134]
VECSEL	SWCNT	0.25	1.23	1074	613	136	DL	[135]
VECSEL	Graphene	0.55	0.466	949	2480	26	808 DL	[136]

[a] τ_p, pulse width.

[b] λ, central wavelength.

[c] f_{rep}, repetition rate.

[d] P_{out}, output power.

[e] AL, argon-ion laser; DL, diode laser; TSL, Ti:sapphire laser; YFL, Yb-doped fiber laser; EDFL, erbium-doped fiber laser; EYFL, Er/Yb-doped fiber laser.

during the inkjet printing process that affect the quality of the devices, including stable jetting of single droplets, appropriate wetting of the substrate, and the uniform distribution of nanomaterials during droplet drying. Hasan *et al.* proposed a binder-free ink formulation by mixing low boiling point alcohols (e.g., ethanol, anhydrous isopropanol, and anhydrous 2-butanol) as solvents. Figure 10(a) is the photograph of the formulated BP ink. The as-prepared binder-free BP ink suppresses coffee ring formation by inducing recirculated Marangoni flow, which supports excellent consistency and spatial uniformity without pre-treatment of the substrates [Figs. 10(b) and 10(c)][161]. Figure 10(d) shows the optical micrograph of printed tracks on Si/SiO_2, glass, and polyethylene terephthalate (PET), confirming that the BP flakes are distributed uniformly without noticeable coffee rings. Self-starting mode-locking was achieved by applying the BP-SA into an EDFL with a fundamental frequency of 31.6 MHz. Figures 10(f)–10(h) display the operation stability of mode-locking by recording every 6 h for 30 days. Later, Zhang's group also reported an inkjet printing BP-SA integrated ultrafast pulse fiber laser. Stretched pulses operating at 1555 nm are generated through intracavity dispersion management with pulse duration of 102 fs, which is ~3 times shorter than the previous results[162]. Then, Zhang *et al.* reported the inkjet printing $Ti_3C_2T_x$ on an SPF for broadband mode-locked lasers[163]. The minimum pulse durations are 215 ps at ~1.06 μm and 114 fs at ~1.5 μm, while the maximum output powers are 14.1 mW and 9.2 mW, respectively. Recently, Hassan *et al.* fabricated inkjet printing MoS_2 optical devices in a large scale for ultrashort pulse (~164.5 fs) generation[158]. The laser output performances are depicted in Figs. 11(b)–11(e). In addition, 3D printing is a technique that deposits materials onto one another in layers to produce a 3D object. For photonic devices, 2D materials based on 3D printing are in the early stage but are still attractive. Lee *et al.* firstly, to the best of our knowledge, reported a filament-based 3D printing technique by printing graphene/polylactic acid onto an SPF for the

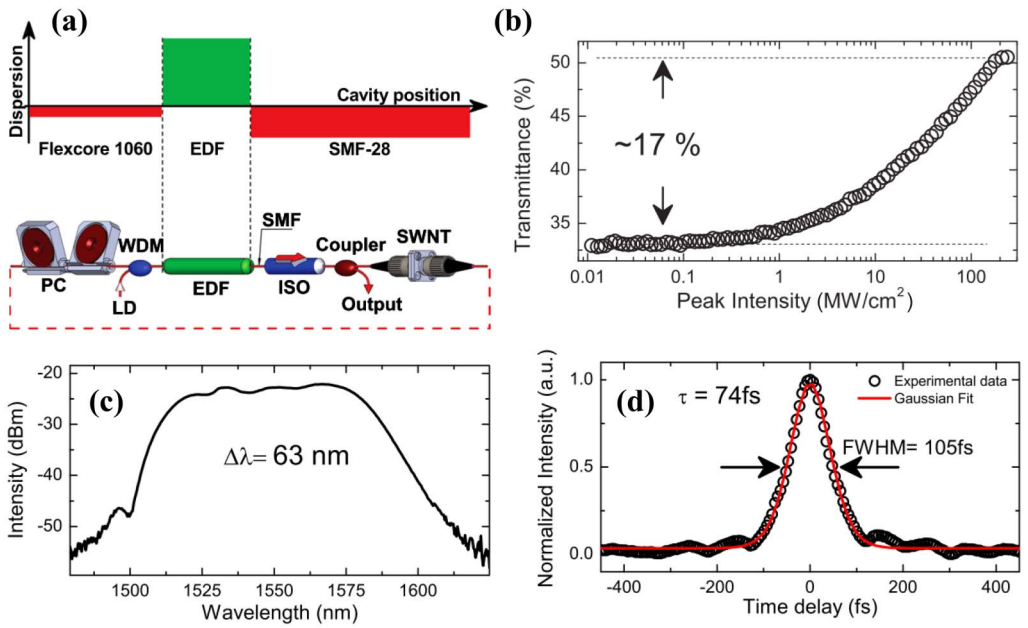

Fig. 7. SWCNT-PVA mode-locked fiber laser with stretched pulse generation. (a) Schematic of the laser setup and the dispersion distribution in the laser cavity. Normal dispersion is provided by the Er-doped fiber (EDF) and anomalous dispersion is provided by the Flexcore 1060 and SMF-28 fibers. WDM, wavelength division multiplexer; SMF, single-mode fiber; ISO, isolator; PC, polarization controller. (b) The nonlinear transmittance of SWCNT-PVA, which gives the modulation depth of 17%. (c) Optical spectrum with the bandwidth of 63 nm. (d) AC trace with a Gaussian fit. (a)–(d) Reproduced with permission[145]. Copyright 2019, American Institute of Physics.

fabrication of low-cost and wideband SAs[164,165]. The measured modulation depths were ~2.2% and ~1.5% at 1.5 μm for the transverse electric (TE) and transverse magnetic (TM) modes, respectively. By applying the SA into an EDFL, stable mode-locked pulses were produced with a pulse duration of 979 fs at a 1560.2 nm central wavelength[164]. Another SA device fabricated by the same approach has also been reported for the 1.9 μm mode-locked fiber laser with the temporal pulse width of 924 fs[165]. Table 3 summarizes the output performances of the passively mode-locked fiber lasers based on SAs fabricated

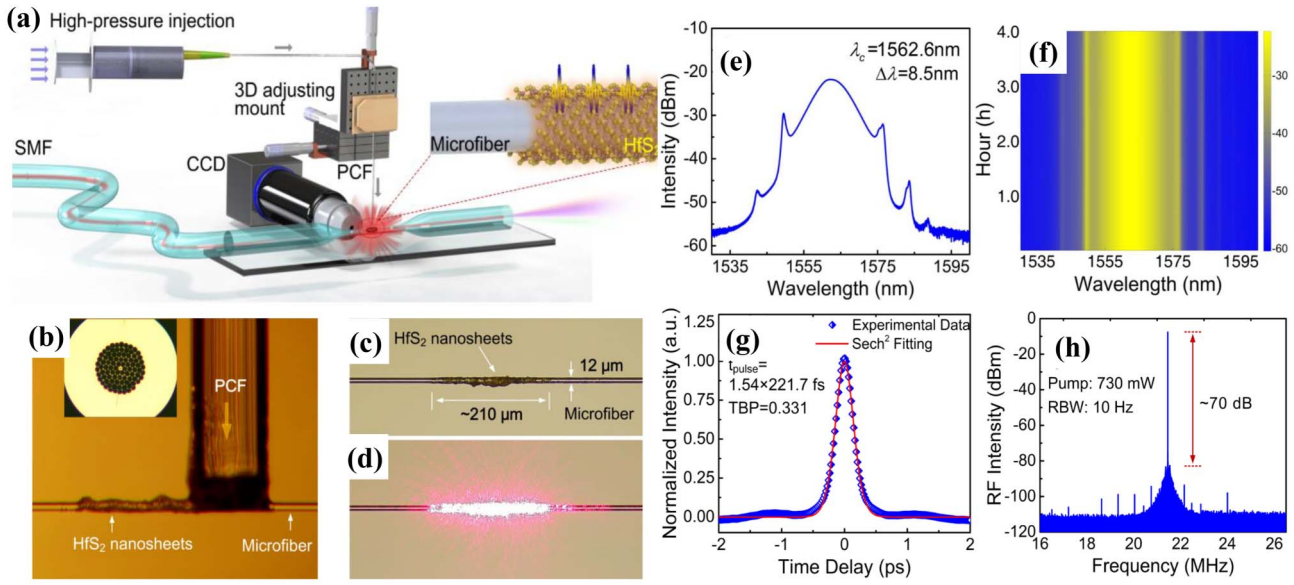

Fig. 8. HfS_2-microfiber SA for mode-locked fiber lasers. (a) Schematic diagram of PCF-assisted HfS_2 deposition system. (b) Picture of the deposition process. Inset displays the end-face of the PCF. Optical microscope images of the HfS_2-microfiber SA (c) before and (d) after launching a 630 nm laser. (e)–(h) Optical characterizations of the laser results. (e) Optical spectrum; (f) optical spectra of soliton operation for 4 h; (g) AC trace; (h) RF spectrum. (a)–(h) Reproduced with permission[155]. Copyright 2018, Wiley-VCH.

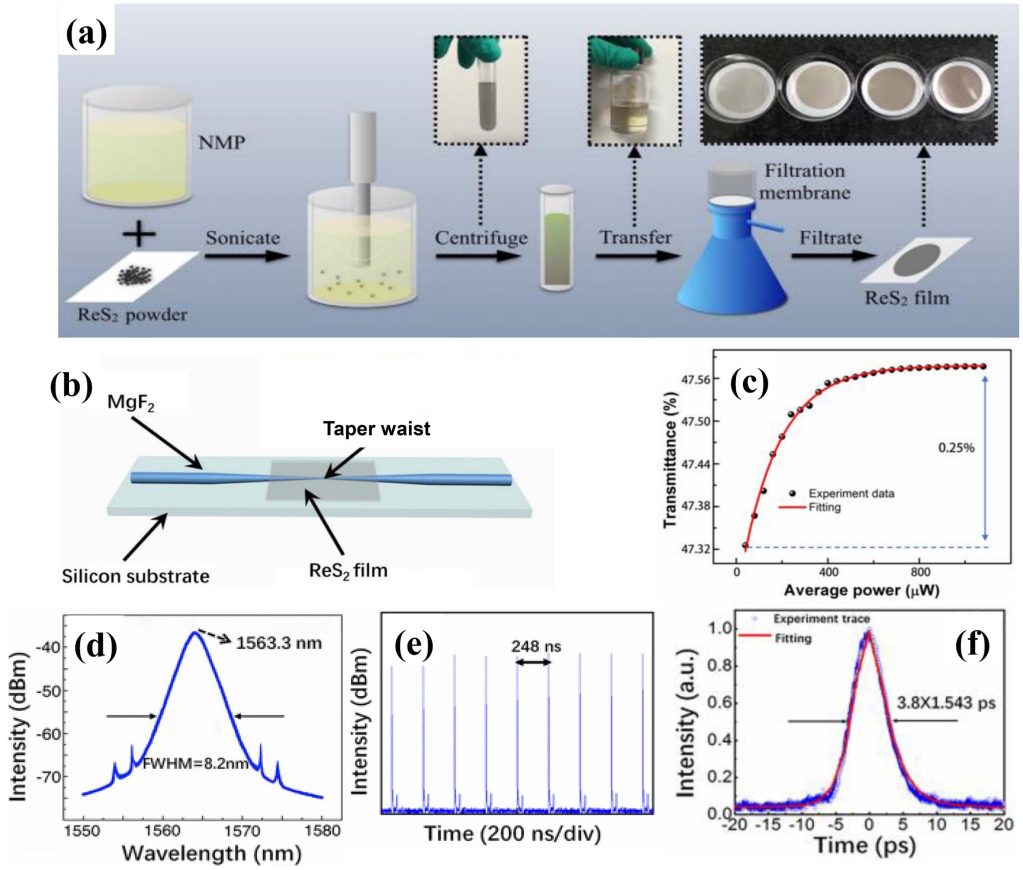

Fig. 9. Ultrafast laser mode-locking with double-covered ReS_2-microfiber (DCRM). (a) Schematic of the ReS_2 film preparation by the vacuum filtration method, which includes sonication, centrifugation, and filtration with different ReS_2 suspension volumes (10 mL, 20 mL, 30 mL, and 40 mL). (b) Schematic of the DCRM where the microfiber is sandwiched between two ReS_2 nanosheet films. The SiO_2 substrate is coated by a MgF_2 layer. (c) Nonlinear transmittance of the DCRM at 1550 nm. (d)–(f) Typical laser characteristics. (d) Optical spectrum, (e) oscilloscope trace, and (f) AC trace. (a)–(f) Reproduced with permission[157]. Copyright 2018, IEEE.

by the LPE technique. For each reference, we quote the best results.

B. PVD technique

Physical vapor deposition (PVD) is a widely used vacuum deposition technique to produce nanometer-thick 2D material films. In a typical PVD process, bulk materials can be vaporized by several techniques, such as bombardment of energic ions [i.e., magnetron sputtering deposition (MSD)], ultraviolet laser ablation [i.e., pulsed laser deposition (PLD)], or heating in a furnace [i.e., thermal evaporation deposition (TED)]. PLD and MSD are the most commonly used transfer-free methods to grow nanomaterial films directly on the target substrates at relatively low working temperature. Those remarkable advantages have motived researchers to re-focus on PVD methods to fabricate the desired SAs on various substrates.

In 2014, our group firstly, to the best of our knowledge, fabricated a novel topological isolator (TI) film on the TF by the PLD technique[192]. The film thickness and crystalline quality can be controlled by varying the deposition conditions, such as laser power density, temperature, and deposition time. The modulation depth of Bi_2Te_3–SA is ~6.7% with a saturation intensity of 26.7 MW/cm^2. By embedding the Bi_2Te_3–SA in to an EDFL, we achieved 286 fs nearly free-chirped soliton pulses at 1560 nm. After that, the Bi_2Te_3 170th harmonic mode-locking (HML) also has been obtained by changing the polarization state and increasing the pump power with the maximum repetition rate of 2.95 GHz[193]. A dissipative soliton mode-locked laser using a Bi_2Te_3–SA also has been reported, generating sub-170 fs pulses with 21 nJ pulse energy[194]. In addition, the Bi_2Te_3–SA has also been applied in a TDFL for ultrashort pulse generation[195]. The $MoTe_2$–SA fabricated by the MSD technique has been proved for stable high-energy soliton mode-locking at 1.5 μm and 2 μm (Fig. 12). The generated pulse duration/pulse energy/average output power were 229 fs/2.14 nJ/57 mW at 1.5 μm and 1.3 ps/13.8 nJ /212 mW at 2 μm, respectively[196]. The pulse energy and output power are the highest among the reported TDFLs using TMDC-SAs. We also fabricated microfiber-based WTe_2–SAs, where the modulation depth, non-saturable loss, and saturation intensity are 31%, 34.3%, and 7.6 MW/cm^2, respectively[197]. Additionally, we have fabricated a novel fiber-integrated WS_2 SAM by sequentially depositing the WS_2 layer and Au film over the fiber end-face (Fig. 13)[198]. The modulation depth, saturation intensity, and reflectivity were measured to be 4.48%, 138 MW/cm^2, and 98%, respectively. The schematic setup of the

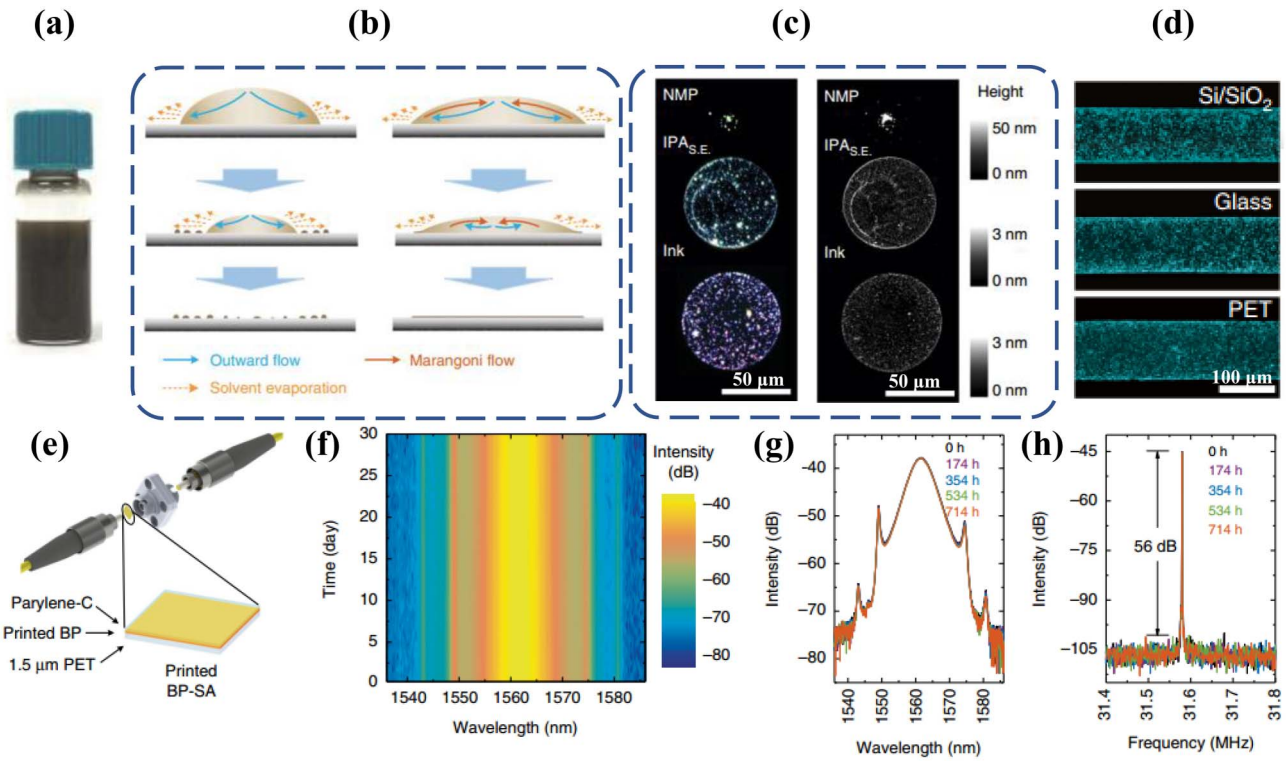

Fig. 10. Ultrafast mode-locked laser using inkjet-printed BP SA. (a) Photograph of formulated BP ink. (b) Droplet drying process without (left) and with (right) introducing recirculated Marangoni flow. (c) Optical photographs (left) and atomic force microscope (AFM) images (right) of the dried droplets. (d) Dark field optical micrographs of the printed tracks on Si/SiO_2, glass, and PET. (e) Printed BP-SA sandwiched between two fiber patch cords. (f) Optical spectra of soliton mode-locking across 30 days. Superposition of the (g) optical spectrum and (h) RF spectrum at the fundamental frequency of 31.6 MHz after 0, 174, 534, and 714 h of operation. (a)–(h) Reproduced with permission[161]. Copyright 2017, Nature.

linear laser cavity is depicted in Fig. 13(a). By incorporating a WS_2-SAM into an EDFL, self-starting mode-locking has been achieved in a wideband range [Figs. 13(b)–13(d)]. After that, high-quality WS_2, MoS_2, WS_2, and gold films were vertically deposited on the fiber end to form a fiber-integrated heterostructure SAM and greatly enhanced the nonlinear optical properties compared with a single-material SAM (Fig. 14)[199]. Figure 14(c) illustrates the band alignment and electron-hole recombination process of the MoS_2–WS_2 heterostructure. The large modulation depth (~16.99 %) and small saturation intensity (~6.23 MW/cm^2) were beneficial for self-starting and pulse shaping in the laser cavity [Fig. 14(d)]. Self-starting mode-locking operation emitting at 1562 nm was realized with excellent laser performance. Table 4 summarizes the results of the passively mode-locked fiber lasers based on the SAs prepared by the PVD technique. For each reference, we quote the best results.

C. CVD technique

Chemical vapor deposition (CVD) is a versatile, scalable, and industry compatible technique for the controllable synthesis of atomic thin LDM films. Until now, a variety of LDMs including graphene, TMDs, and TIs have been synthesized in the lab[206–218]. The first, to the best of our knowledge, CVD-graphene mode-locking was reported by Bao *et al.* in 2009, which demonstrated the generation of 756 fs pulses at the telecommunication band[62]. Sobon *et al.* firstly, to the best of our knowledge, reported a comprehensive study on the nonlinear optical properties of graphene by changing the layer number, which demonstrated that the modulation depth scales with the number of layers[59]. Apart from graphene, other nanomaterials (e.g., MoS_2, WS_2, Bi_2Se_3, $MoSe_2$, WSe_2, $PtSe_2$, and ReS_2) combined with different optical configurations also have been reported for ultrafast laser applications, which are shown in Table 5. CVD grown WSe_2 film with high crystalline quality has been transferred onto the microfiber to form a hybrid SA for broadband mode-locking[215]. Figures 15(b) and 15(c) are SEM images of the WSe_2–SA, where a large-area WSe_2 film is tightly clinging to the waist of the TF. Stable soliton mode-locking has been achieved with the shortest pulse durations of 477 fs (at 1.5 μm) and 1.18 ps (at 2 μm). The obtained saturable absorption properties and laser performances with different CVD materials are summarized in Table 5.

3.2.3. LDMs for MIR fiber lasers

MIR (2–10 μm) laser sources are of particular interests for various applications due to the unique fingerprint molecule spectra and transparent atmosphere windows in this region. Owing to the water vapor absorption in the atmosphere, which will induce

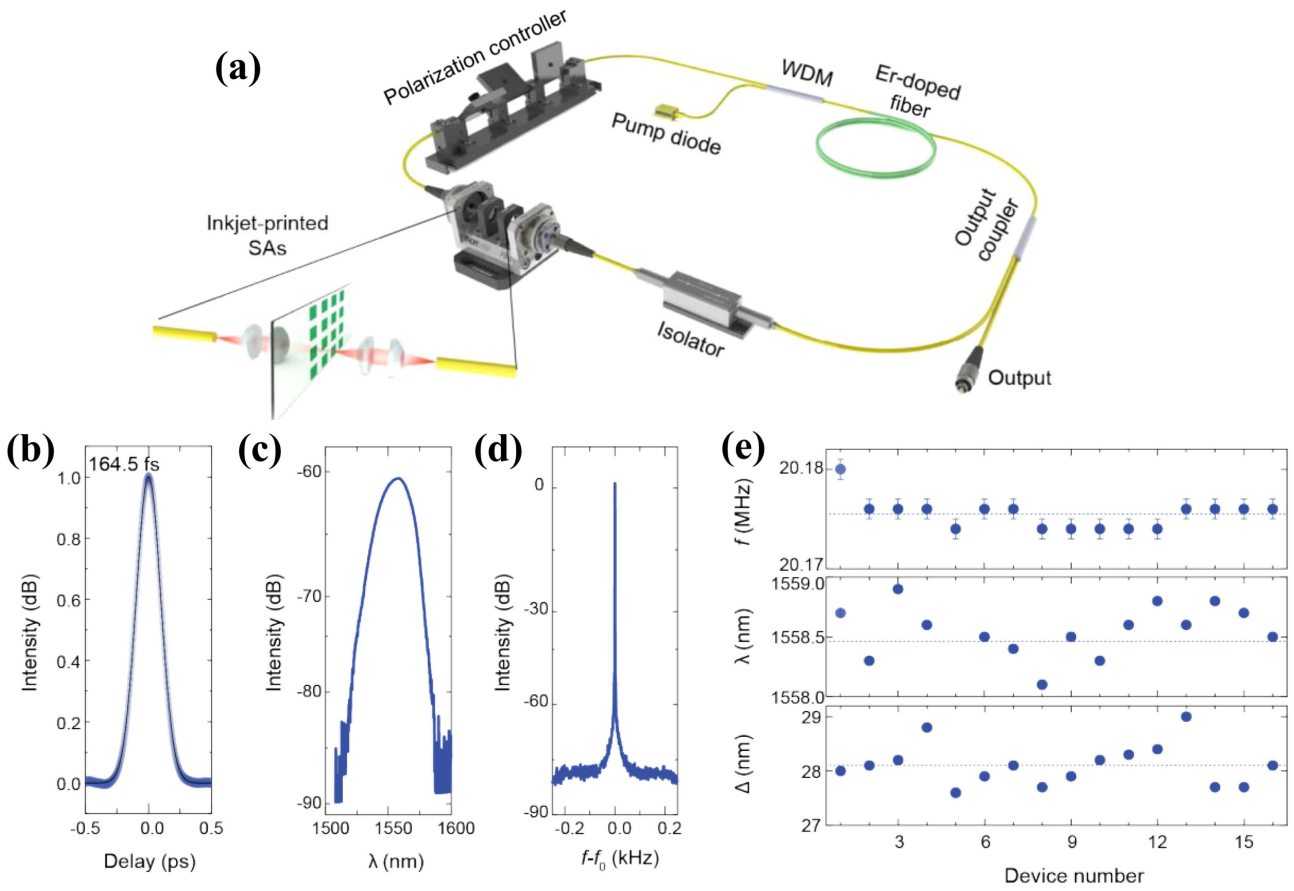

Fig. 11. Ultrafast mode-locking with inkjet-printed 2 H–MoS_2 optical devices. (a) Schematic picture of the EDFL cavity. (b) AC trace fitted with a Gaussian curve. (c) Output laser spectrum and (d) RF spectrum at a fundamental frequency of 20.176 MHz. (e) Measured fundamental frequency (top), central wavelength (medium), and FWHM bandwidth (down) generated from 16 individual 2H–MoS_2 SAs. (a)–(e) Reproduced with permission[158]. Copyright 2020, American Association for the Advancement of Science.

considerable non-saturable loss, all-solid-state lasers around or after 2.8 μm have not been realized yet. Fiber lasers, hence, display their unique superiority for mode-locking in this region. Fluoride fiber lasers (FFLs) with various cavity structures, gain fibers, and SAs have been realized in the 2.8–3.5 μm region[219–225]. In 2015, Jiang *et al.* reported an MIR mode-locked FFL based on Bi_2Te_3 nanosheets, which displays a promising application of LDMs for ultrafast lasers at 2830 nm[220]. CW mode-locking was observed with repetition rate of 10.4 MHz and pulse width of 6 ps. In 2016, Qin *et al.* firstly, to the best of our knowledge, demonstrated the Er:ZBLAN mode-locked fiber laser around 2.8 μm utilizing a BP-SAM[221]. In 2018, they also reported the first, to the best of our knowledge, 2.8 μm all-fiber mode-locking with BPs[223]. Different from most solid-state lasers, FFLs require large modulation depths to initiate and sustain stable mode-locking operations. One effective method is to increase the sample thickness. Subsequently, Qin *et al.* reported a dual-wavelength pumped mode-locked Er-doped FFL at 3.5 μm with a bulk BP-SAM[224]. The output power was 40 mW with the pulse duration estimated to be tens of picoseconds. Recently, they demonstrated pulse energy and peak-power scaling of MIR FFLs by dispersion management[225]. The mode-locked FFL produced 215 fs pulses with pulse energy of 9.3 nJ and peak power of 43.3 kW.

4. Discussion

As far as the reported results are concerned, the performance of SESAMs and LDM-SAs has improved steadily. The fabrication of SAs is improving toward being controllable, low cost, easy integration as well as mass production. Meanwhile, the operating bands of SAs are developing toward MIR and far-infrared wavelengths. To ensure further advance of SAs, there are several basic requirements for SAs. (1) Self-starting ability: the SA is required to achieve mode-locking immediately after being inserted into a laser cavity without introducing perturbations. (2) Durability: in order to achieve the long-term mode-locking operation under high pump power, the as-fabricated SAs should possess a higher damage threshold as well as a lower non-saturable loss. (3) Ultrafast recovery time: SAs with ultrafast recovery time are more capable of achieving shorter pulse widths.

Table 3. Passively Mode-Locked Fiber Lasers Based on LPE-SAs..

			SA properties[c]			Laser performances[d]				
Materials	Integration method[a]	λ (nm)[b]	α_s (%)	I_s (MW·cm^{-2})	α_{ns} (%)	τ (fs)	f_{rep} (MHz)	P (mW)	SNR (dB)	Ref.
SWCNT	Sandwiched	1030	15	\	44	235	50	155	\	[166]
SWCNT	Sandwiched	1030	52.7	2.512	51	175	21.2	8.68	63	[167]
SWCNT	Sandwiched	1550	17	203	\	74	33	1.2	76	[145]
CNT	Sandwiched	1928.5	13.3	\	\	501	56.368	28.5	>70	[168]
SWCNT	Sandwiched	1560	16.9	18.9	\	113	18.76	12.8	77	[169]
SWCNT	SPF	1563	\	\	\	1020	38.9	250	\	[152]
CNT	FP mirror	1563	5	2.5	\	790	19,450	\	27	[170]
SWCNT	Sandwiched	1927	10	68	14	152	25.76	4.85	73	[171]
Graphene	Sandwiched	1560	2	337	28	174	27.4	\	87.4	[172]
Graphene	Sandwiched	1550	\	\	\	263	18.67	0.68	63	[173]
Graphene	Sandwiched	1558	2	100	70	268	27.4	1.2	87.4	[174]
Graphene	FP mirror	1562	\	\	\	865	9670	\	40	[175]
MoS_2	Sandwiched	979	3.6	6.3	6.3	13,000	26.5	16.7	60	[176]
MoS_2	TF	1556.86	2.82	\	57.34	3000	2500	5.39	\	[153]
MoS_2	Sandwiched	1569.5	4.3	34	24	710	12.09	1.78	60	[177]
WS_2	Sandwiched	1572	2.9	370	30.9	919	25.3	\	75	[178]
WS_2	SPF	1557	11	5	18	660	10.2	\	65	[179]
WS_2	TF	1566	0.14	\	82	467	21.1	0.32	60.8	[180]
WS_2	TF	1561	0.5	\	21.4	369	24.93	1.93	69	[181]
WSe_2	SPF	1556.7	0.3	\	\	1310	3252.65	19	\	[182]
$MoSe_2$	Sandwiched	1560	7.3	\	\	580	8.8	218	50	[183]
ReS_2	Sandwiched	1557	0.12	74	\	1600	5.48	0.4	\	[184]
SnS_2	Sandwiched	1562	4.6	125	13.6	623	29.33	1.2	45	[185]
Bi_2Se_3	Sandwiched	1557	3.9	12	68	660	12.5	1.8	55	[186]
Bi_2Te_3	Sandwiched	1557	2	180	34	1080	8.64	0.11	60	[187]
Bi_2Te_3	TF	1560	1.82	\	67	2180	3125	\	\	[188]
Bi	TF	1561	5.6	48.2	62.3	193	8.8	5.6	55	[189]
BP	Sandwiched	1560.5	4.6	\	48	272	28.2	0.5	65	[190]
BP	Sandwiched (printed)	1555	10.03	14.98	9.97	102	23.9	1.7	60	[162]
BP	Sandwiched (printed)	1562	\	\	\	605	31.6	\	56	[161]
TiS_2	Sandwiched	1569.5	62	1210	\	1040	5.34	\	66	[191]
GaTe	TF	1563.17	42.3	\	7.1	408	36.5	13.2	80	[154]
GeTe	TF	1931.51	8.3	\	76.7	983	35	16.2	87.6	[154]

(Continued)

Table 3. (Continued)

Materials	Integration method[a]	λ (nm)[b]	SA properties[c]			Laser performances[d]				Ref.
			α_s (%)	I_s (MW·cm^{-2})	α_{ns} (%)	τ (fs)	f_{rep} (MHz)	P (mW)	SNR (dB)	
HfS_2	TF	1561.8	15.7	8	20.6	221.7	21.45	89.4	68	[155]
$HfSe_2$	TF	1561.4	5.8	163.2	45.6	297	18.09	48.5	80	[156]
$AuTe_2Se_{4/3}$	Sandwiched	1557.53	65.58	0.089	18.83	147.7	69.93	21.4	91	[150]
Ti_3CN	SPF	1557	1.7	\	\	660	15.4	0.05	60	[160]

[a]TF, tapered fiber; SPF, side-polished fiber; FP mirror, Fabry-Perot mirror.

[b]λ, central wavelength.

[c]α_s, saturable absorbance; I_s, saturation intensity; α_{ns}, non-saturable absorbance.

[d]τ, pulse width; f_{rep}, repetition rate; P, output power; SNR, signal-to-noise ratio.

(4) Low-cost and controllable fabrication are important factors for industry compatibility.

SESAMs with good customization have been widely employed in commercial lasers. In the past few decades, many researches have been done to improve the performance of SESAMs. The development of VECSEL and MIXSEL chips has greatly simplified the cavity structures, which allow for generating GHz repetition rates and several kilowatts peak power directly from a laser cavity. However, a retaining limitation of SESAMs is inflexible, which does not meet the characteristics of all-fiber integration. In addition, SESAMs have limited bandwidth (< 100 nm) and function wavelengths (800–2500 nm) due to the lack of effective materials.

LDMs with features like flexibility and ultrafast and broadband photoresponsivity are considered to meet these requirements. Figure 16 summarizes the mode-locked pulse width with different SAs in wide operating wavelength ranges. We use several colors to distinguish different SA fabricating technologies. LPE is a simple, contactless micromechanical exfoliation technique for high-yield nanosheets production. However, there are glaring problems such as poor fabrication controllability and repeatability and mode-locking performance degradation for a

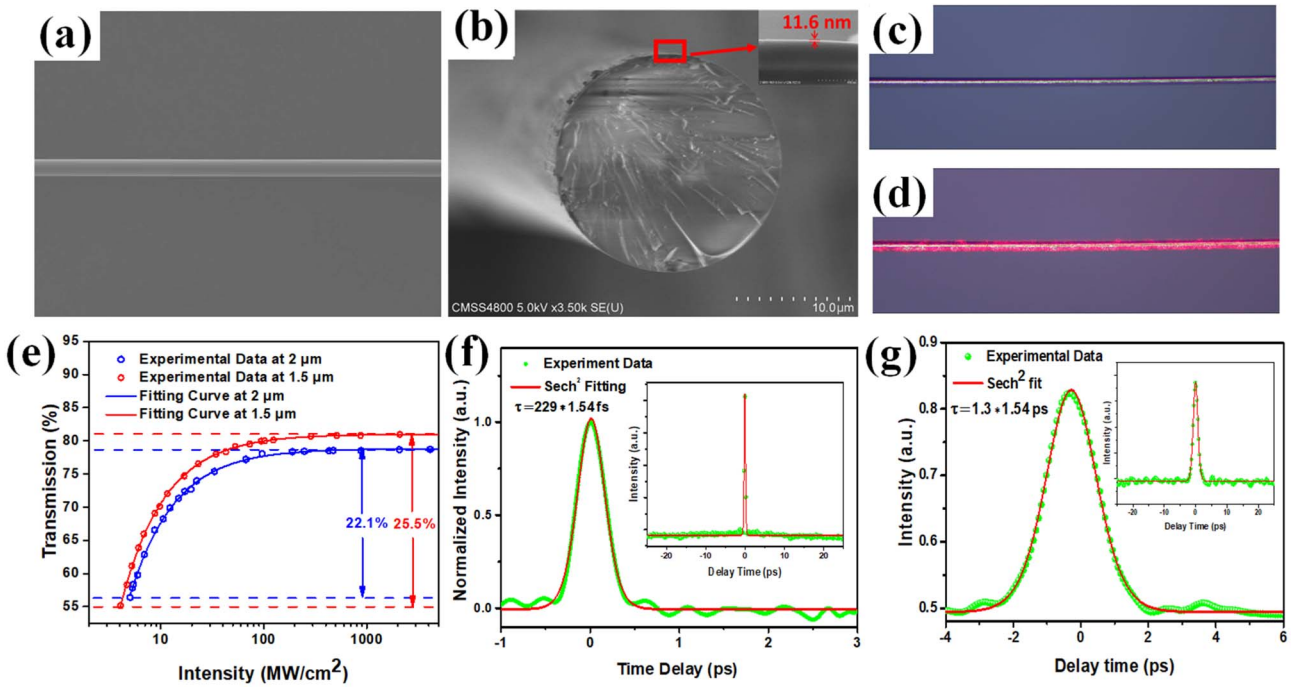

Fig. 12. High-energy soliton pulse generation by magnetron sputtering deposition (MSD) grown $MoTe_2$-microfiber SA. (a) SEM image of the microfiber coated with $MoTe_2$ film and (b) cross-section view of the $MoTe_2$-microfiber. Microscope image of the $MoTe_2$-microfiber (c) without and (d) with guiding a red light. (e) Nonlinear transmittance properties of $MoTe_2$ SA at 1.5 μm and 2 μm. AC traces at (f) 1.5 μm and (g) 2 μm, respectively. (a)–(g) Reproduced with permission[196]. Copyright 2018, Chinese Laser Press.

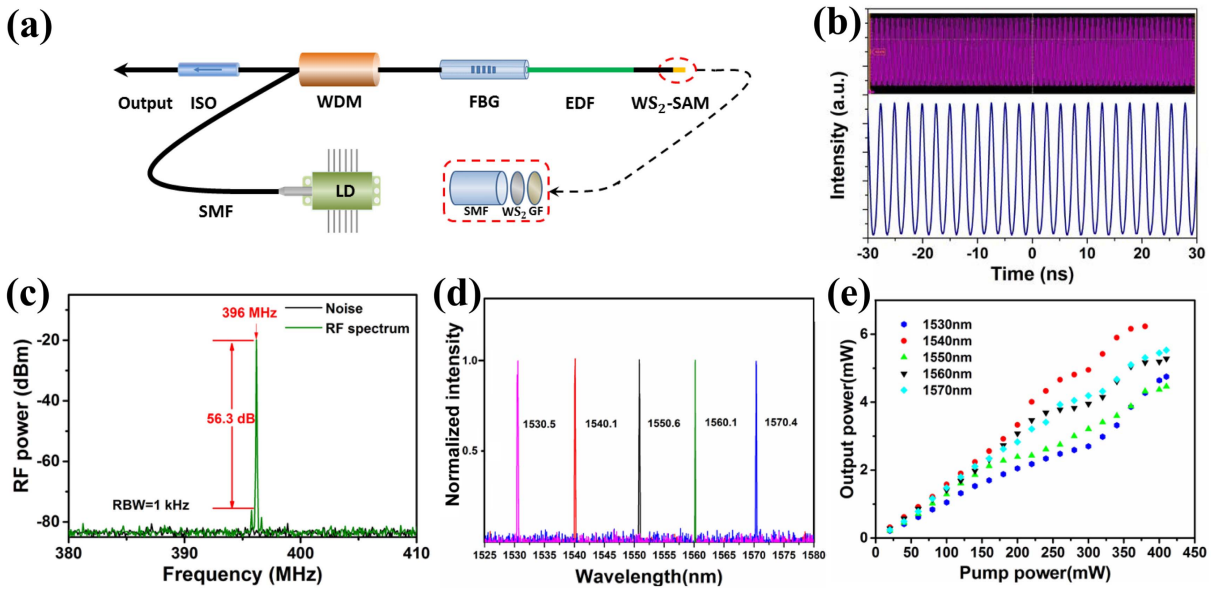

Fig. 13. Self-starting mode-locking by fiber-integrated WS_2-SAM. (a) Schematic picture of mode-locked fiber laser cavity. (b)–(e) Mode-locked laser performances. (b) Oscilloscope trace; (c) RF spectrum with a fundamental frequency of 396 MHz; (d) laser spectra using different fiber Bragg gratings (FBGs); (e) laser slope efficiencies under different operating wavelengths. (a)–(e) Reproduced with permission[198]. Copyright 2015, IEEE.

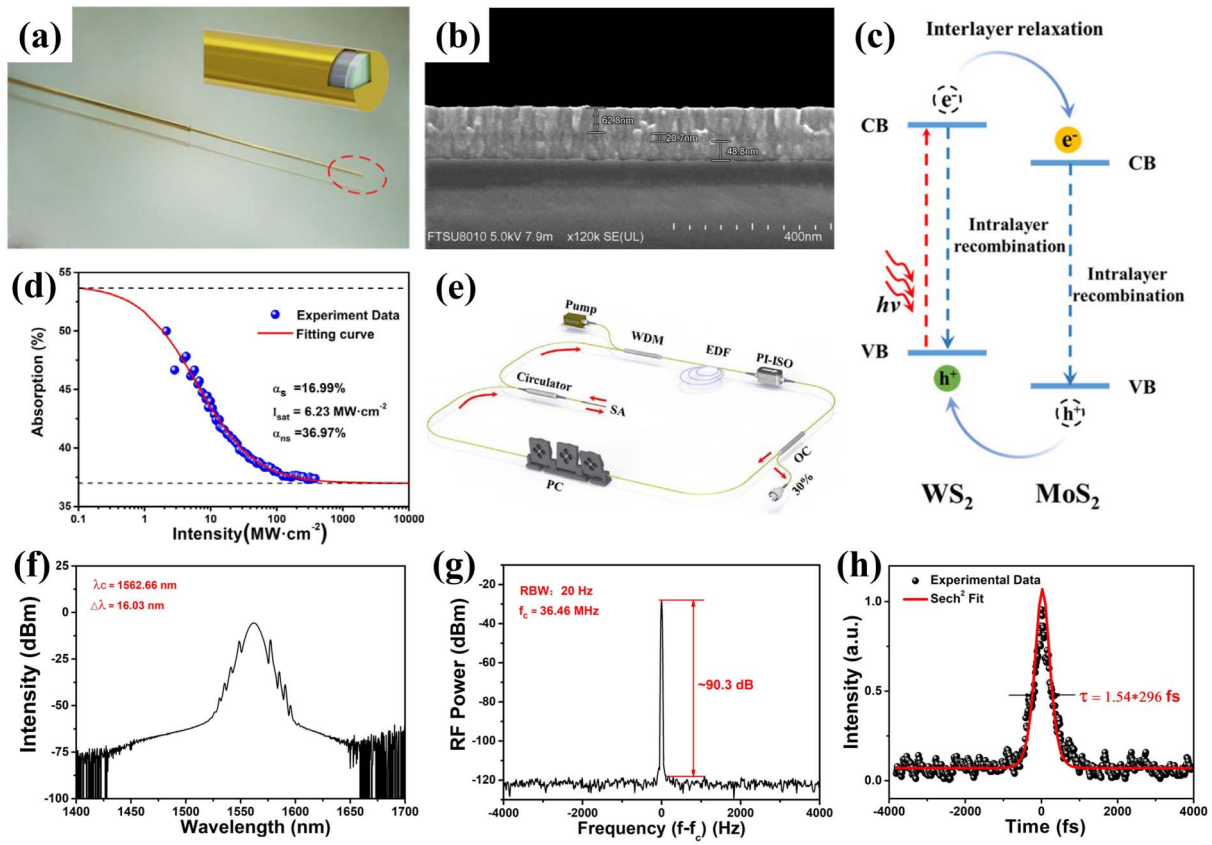

Fig. 14. WS_2–MoS_2–WS_2 heterostructure SAM for mode-locked fiber lasers. (a) Schematic image of the fiber-integrated heterostructure SA. (b) SEM image of the measured lateral thickness (48.4/20.7/62.8 nm) on a silicon wafer. (c) The predicted band structure of MoS_2–WS_2 heterostructure with a type II heterojunction. CB is the conduction band, and VB is the valence band. (d) Nonlinear optical absorption of the heterostructure SA. (e) Illustration of a typical EDFL cavity. (f) Output laser spectrum. (g) AC trace of the output pulse. (h) RF spectrum. (a)–(h) Reproduced with permission[199]. Copyright 2017, Optical Society of America.

Table 4. Passively Mode-Locked Fiber Lasers Based on PVD-SAs..

Materials	Integration method[a]	λ (nm)[b]	SA Properties[c]			Laser Performances[d]				Ref.
			α_s (%)	I_s (MW·cm^{-2})	α_{ns} (%)	τ (fs)	f_{rep} (MHz)	P (mW)	SNR (dB)	
Bi_2Te_3	TF	1562.4	6.2	28	20	320	2950	45.3	75	[193]
Bi_2Te_3	TF	1930.07	38	3.3	31.2	1240	14.51	130	84	[195]
Bi_2Te_3	TF	1542	7.42	175	\	70	95.4	63	65	[200]
Bi_2Te_3	SPF	1047.1	0.5-2.9	\	\	5900	19.28	4	71	[201]
Bi_2Te_3	SPF	1558	5.3-13	\	\	167	25.38	5.34	68	[194]
WTe_2	TF	1915.5	31	7.6	34.3	1250	18.72	39.9	95	[197]
$MoTe_2$	TF	1559.57	25.5	9.6	19.1	229	26.6	57	93	[196]
		1934.85	22.1	12.3	21.3	1300	15.37	212	84	[196]
α-In_2Se_3	TF	1565	4.5	7.3	21.9	276	40.9	83.2	90	[202]
		1932	6.9	10.6	28.8	1020	15.8	112.4	90	[202]
WS_2	TF	1559.7	1.2	25	\	452	1040	11.3	48	[203]
WS_2	SAM	1549.98	4.48	138	2	\	396	6.2	56.3	[198]
$WS_2/MoS_2/WS_2$	SAM	1562.66	16.99	6.23	36.97	296	36.46	25	90.3	[199]
MoS_2-Bi_2Te_3-MoS_2	SAM	1554	64.17	151.176	35.83	286	36.4	20	73	[204]
Cd_3As_2	Sandwiched	1968.5	3.5	12	\	1360	23.2	4.9	70	[205]
		1560	5.1	67	\	920	17.6	0.7	70	[205]

[a]TF, tapered fiber; SPF, side-polished fiber; SAM, saturable absorber mirror.

[b]λ, central wavelength.

[c]α_s, saturable absorbance; I_s, saturation intensity; α_{ns}, non-saturable absorbance.

[d]τ, pulse width; f_{rep}, repetition rate; P, output power; SNR, signal-to-noise ratio.

long-term operation, which should not be neglected. Notably, the inkjet printing method provides a new platform for the mass production of SA devices, and the long-term operation with high stability can be achieved by encapsulating SAs with a hexagonal boron nitride (h-BN) layer. Another advantage of inkjet printing is the controllable printing of desired graphic arrays on a myriad of substrates, which has already been applied in various photoelectronic devices (e.g., ultrafast lasers, photodetectors, and wearable electronic devices).

PVD is a transfer-free method to grow nanomaterials directly on the target substrates at relatively low working temperatures. The deposited films generally have good crystallinity after annealing. For fiber-end-face-integrated SAMs, selecting materials with an appropriate modulation depth is critical for self-starting mode-locking. This compact SA device with a protective gold layer can be applied for stable high-frequency (~GHz) mode-locking. CVD fabricated SAs possess a low damage threshold due to the atomic thickness and cannot work steadily for long periods of time without encapsulation. In addition, the additional transfer processes to the target substrate are prone to introducing undesired physical damages or defects, causing higher non-saturable losses. Polymer as an auxiliary is often added during the transfer process. Rapid and residue-free transfer of CVD synthesized films is still a challenge so far.

5. Outlook

5.1. New SA structures

Different atomically thin 2D materials can be readily stacked together by van der Waals forces to form a heterostructure, which offers a flexible and easy approach for bandgap engineering. In comparison with a single material, the heterostructure exhibits excellent nonlinear optical properties due to strong interlayer coupling[226]. Take the type-II WS_2–MoS_2 heterojunction as an example; the photo-excited electrons and holes prefer to stay at the bottom of the conduction band and the top of the valence band, which can lead to an ultrafast carrier

Table 5. Passively Mode-locked Fiber Lasers Based on CVD-SAs.

			SA properties[c]			Laser performances[d]				
Materials	Integration method[a]	λ (nm)[b]	α_s (%)	I_s (MW·cm^{-2})	α_{ns} (%)	τ (fs)	f_{rep} (MHz)	P (mW)	SNR (dB)	Ref.
Graphene	Sandwiched	1545	11	\	~64	88	21.15	1.5	65	[206]
Graphene	Sandwiched	1884	0.4	\	\	1200	20.5	1.35	~70	[207]
Graphene	TF	1550	12	40	27	970	8.57	\	65	[208]
MoS_2	Sandwiched	1568.9	35.4	0.35	34.1	1280	8.288	5.1	62	[209]
MoS_2	Sandwiched	1569.6	\	\	\	1420	216	6.81	36.1	[70]
WS_2	Sandwiched	1568.3	15.1	157.6	45.9	1490	0.487	62.5	71.8	[210]
WS_2	TF	1565	0.5	\	\	332	31.11	\	81.6	[211]
$MoSe_2$	TF	1552	22.57	7.747	46.46	207	64.56	\	85	[212]
WSe_2	Sandwiched	1562	52.38	1.399	45.51	185	58.8	30	95	[213]
WSe_2	TF	1863.96	1.83	3.7	87	1160	11.36	32.5	53	[214]
WSe_2	TF	1556.42	54.5	2.97	~10	477	14.02	\	80	[215]
WSe_2	TF	1886.22	1.83	\	~90	1180	11.36	32.5	80	[215]
$MoTe_2$	TF	1930.22	5.7	8.3	70	952	14.353	36.7	87.8	[216]
$PtSe_2$	TF	1563	4.9	340	~70	1020	23.3	\	61	[217]
Bi_2Se_3	Sandwiched	1557.9	15	6.59	\	\	1.71	82.6	42	[218]

[a]TF, tapered fiber.

[b]λ, central wavelength.

[c]α_s, saturable absorbance; I_s, saturation intensity; α_{ns}, non-saturable absorbance.

[d]τ, pulse width; f_{rep}, repetition rate; P, output power; SNR, signal-to-noise ratio.

lifetime. A previous report has verified that the intralayer recombination of single-layer MoS_2 is 2 ps, while it is 50 fs in a WS_2–MoS_2 heterostructure[227]. Additionally, due to the similar crystalline structure and lattice constants, the interfaces between MoS_2 and WS_2 could be bonded with minimal structural defects[228]. So far, 2D heterojunctions have been implemented in various optical and optoelectronics devices that are not limited to ultrafast lasers but are also in field-effect transistors, photodetectors, sensors, and light-emitting diodes[229,230]. As mentioned earlier, Chen *et al.* have fabricated a MoS_2–WS_2–MoS_2 heterojunction by the MSD technique on the tip of a single-mode fiber (SMF)[199]. Liu *et al.* have also reported MoS_2–WS_2 heterojunctions as a useful SA for ultrafast pulses generation[231]. The remarkable nonlinear optical properties are observed with a large modulation depth (~19.12%) and lower saturation intensity (1.361 MW/cm^2). Heterojunctions by mechanically stacking different CVD grown 2D materials have also been reported for ultrafast lasers[232,233]. Mechanical stacking of 2D materials does not necessarily lead to strong interlayer coupling, which needs proper thermal annealing to reduce the interlayer distance. In general, 2D material heterojunctions with specific structure design show great potential for applications that are in their budding period.

Metasurfaces, artificial materials made of subwavelength elementary cells, have emerged as promising platforms for unexpected physical properties generation. Recently, Wang *et al.* demonstrated that plasmonic gold metasurfaces with excellent saturable absorption properties could behave as reliable SAs[234]. This saturable metasurfaces material provides an idea to further increase the modulation depth and decrease the saturation intensity. Thus, saturable plasmonic metasurfaces offer a high degree of freedom to design novel ultrathin and efficient SAs for the desired optical performances.

5.2. Actively controllable devices

Active manipulation of light in an optical fiber has gained research interest due to its compatibility with numerous optical systems. In 2015, Lee *et al.* demonstrated an electronically tunable all-fiber graphene device by fabricating graphene-based field effect transistor (FET) on the SPF[235]. *Q*-switching and mode-locking were realized by applying the tunable

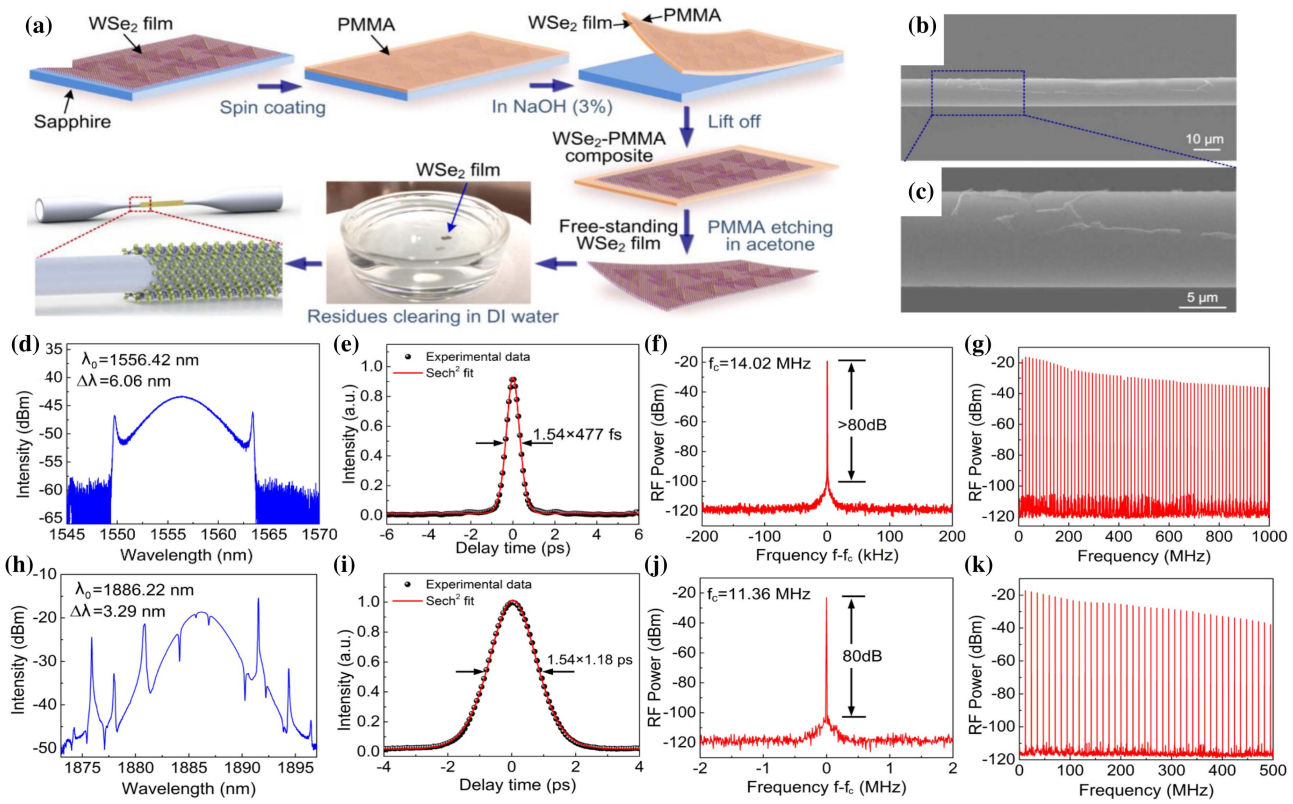

Fig. 15. Broadband mode-locked fiber laser by a large-area WSe_2 film. (a) Schematic image of the microfiber-integrated WSe_2–SA fabrication process by transferring the CVD grown WSe_2 film onto the TF. (b) SEM image of the microfiber coated with the WSe_2 film. (c) Magnified SEM image of the marked area in (b). (d)–(g) Mode-locked characteristics of the EDFL. (d) Optical spectrum; (e) AC trace; (f) RF spectrum; (g) RF spectrum in broad bandwidth. (h)–(k) Output laser performances of the TDFL. (h) Optical spectrum; (i) AC trace; (j) RF spectrum; (k) wideband RF spectrum. (a)–(k) Reproduced with permission[215]. Copyright 2017, Optical Society of America.

graphene-SA in a laser system. This can also be extended to photodetectors, optical waveguides, and other photonic devices. In addition, a graphene-based active mode-locker has been reported by Sun's group for electrically controlled broadband high repetition rate operation[236]. This device provides a more compact, cost-effective, and robust active mode-locking solution. This research also provides a new idea for GHz pulse generation using 2D materials with high modulation depths (particularly, 2D heterostructures). A novel all-fiber integration electro-optic modulator was reported recently, where the graphene film was directly grown on the hollow holes and the outside wall of the PCF by the CVD technique with the growing length up to half a meter[237]. This electro-optic modulator exhibits a strong light–matter interaction, which would inspire the generation of novel electrically tunable fiber devices such as all-fiber mode-locking lasers, nonlinear converters, and optical limiters. The exploration of actively tunable SAs is in its infancy, which is of great significance for promoting the development of active optical devices.

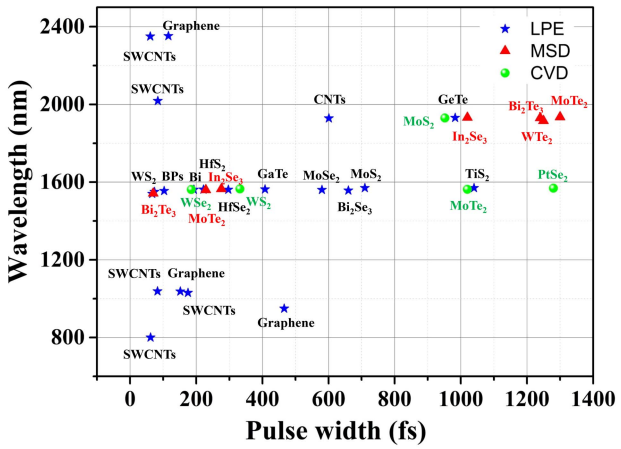

Fig. 16. Wide-spectral mode-locking with different 2D materials.

5.3. SAs for MIR wavelength

During the past two decades, various SAs have been adopted for FFL mode-locking. However, the output pulse durations were several to tens of picoseconds with low average powers. Mode-locking in the fs range around 2.8 μm was achieved by nonlinear polarization rotation (NPR) in 2015[238,239]. LDMs with broadband absorption and ultrafast recovery time have been reported for CW mode-locking in the MIR region, whereas the pulse width still remains at the picosecond scale.

So far, no fs mode-locked FFL at 3.5 μm has been reported. The gapless electronic structures of topological Dirac semimetals (e.g., Cd_2As_3) endow them with broadband saturable absorption effects, which can be used as potential SAs for MIR mode-locking[240].

In summary, the overall development of SAs tends to compactness, controllable fabrication, and scalability as well as active controllability. It is crucial to put emphasis on SAs that are fully compatible with fiber lasers, which play an increasingly important role in industry and human life. The fabrication of reliable and effective SAs will open up new directions for mass production of next-generation lasers.

Acknowledgement

This work was supported by the National Natural Science Foundation of China (Nos. 61905148, 61775146, and 12074264) and the Shenzhen Science and Technology Project (Nos. JCYJ20190808160205460, JCYJ20190808174201658, and JCYJ20190808141011530).

References

1. T. H. Maiman, "Stimulated optical radiation in ruby," Nature **187**, 493 (1960).
2. A. Javan, W. R. Bennett, and D. R. Herriott, "Population inversion and continuous optical maser oscillation in a gas discharge containing a He-Ne mixture," Phys. Rev. Lett. **6**, 106 (1961).
3. E. Snitzer, "Optical maser action of Nd^{+3} in a barium crown glass," Phys. Rev. Lett. **7**, 444 (1961).
4. R. N. Hall, G. E. Fenner, J. D. Kingsley, T. J. Soltys, and R. O. Carlson, "Coherent light emission from GaAs junctions," Phys. Rev. Lett. **9**, 366 (1962).
5. W. Dietel, E. Döpel, D. Kühlke, and B. Wilhelmi, "Pulses in the femtosecond range from a cw dye ring laser in the colliding pulse mode-locking (CPM) regime with down-chirp," Opt. Commun. **43**, 433 (1982).
6. U. Morgner, F. X. Kärtner, S. H. Cho, Y. Chen, H. A. Haus, J. G. Fujimoto, E. P. Ippen, V. Scheuer, G. Angelow, and T. Tschudi, "Sub-two-cycle pulses from a Kerr-lens mode-locked Ti:sapphire laser," Opt. Lett. **24**, 411 (1999).
7. M. T. Asaki, C. P. Huang, D. Garvey, J. Zhou, H. C. Kapteyn, and M. M. Murnane, "Generation of 11-fs pulses from a self-mode-locked Ti: sapphire laser," Opt. Lett. **18**, 977 (1993).
8. A. Stingl, M. Lenzner, C. Spielmann, F. Krausz, and R. Szipöcs, "Sub-10-fs mirror-dispersion-controlled Ti:sapphire laser," Opt. Lett. **20**, 602 (1995).
9. P. Antoine, A. L'huillier, and M. Lewenstein, "Attosecond pulse trains using high-order harmonics," Phys. Rev. Lett. **77**, 1234 (1996).
10. K. T. Kim, C. M. Kim, M. G. Baik, G. Umesh, and C. H. Nam, "Single sub 50 attosecond pulse generation from chirp-compensated harmonic radiation using material dispersion.," Phys. Rev. A **69**, 051805 (2004).
11. A. V. Korzhimanov, A. A. Gonoskov, E. A. Khazanov, and A. M. Sergeev, "Horizons of petawatt laser technology," Phys.-Uspekhi **54**, 9 (2011).
12. F. Lureau, G. Matras, S. Laux, C. Radier, O. Chalus, O. Casagrande, C. Derycke, S. Ricaud, P. Calvet, L. Boudjemaa, C. S. Boisson, D. Ursescu, and I. Dancus, "10 petawatt laser system for extreme light physics," in *Laser Congress 2019* (2019), paper ATh1A.5.
13. A. H. Zewail, "Laser femtochemistry," Science **242**, 1645 (1988).
14. H. Jung, R. Stoll, X. Guo, D. Fischer, and H. X. Tang, "Green, red, and IR frequency comb line generation from single IR pump in AlN microring resonator," Optica **1**, 396 (2014).
15. M. Suh, Q. Yang, K. Y. Yang, X. Yi, and K. J. Vahala, "Microresonator soliton dual-comb spectroscopy," Science **354**, 600 (2016).
16. J. Wu, Y. Xu, J. Xu, X. Wei, A. Chan, A. Tang, A. Lau, B. Chung, H. Shum, E. Lam, K. Wong, and K. Tsia, "Ultrafast laser-scanning time-stretch imaging at visible wavelengths," Light Sci. Appl. **6**, e16196 (2017).
17. M. Hassan, J. Baskin, B. Liao, and A. H. Zewail, "High-temporal-resolution electron microscopy for imaging ultrafast electron dynamics," Nat. Photon. **11**, 425 (2017).
18. K. Sugioka and Y. Cheng, "Ultrafast lasers—reliable tools for advanced materials processing," Light Sci. Appl. **3**, e149 (2014).
19. G. B. Rieker, F. R. Giorgetta, W. C. Swann, J. Kofler, A. M. Zolot, L. C. Sinclair, E. Baumann, C. Cromer, G. Petron, C. Sweeney, P. P. Tans, I. Coddington, and N. R. Newbury, "Frequency-comb-based remote sensing of greenhouse gases over kilometer air paths," Optica **1**, 290 (2014).
20. A. Rohrbacher, O. E. Olarte, V. Villamaina, P. L. Alvarez, and B. Resan, "Multiphoton imaging with blue-diode-pumped SESAM-modelocked Ti: sapphire oscillator generating 5 nJ 82 fs pulses," Opt. Express **25**, 10677 (2017).
21. U. Keller, "Recent developments in compact ultrafast lasers," Nature **424**, 831 (2003).
22. O. Okhotnikov, A. Grudinin, and M. Pessa, "Ultra-fast fiber laser systems based on SESAM technology: new horizons and applications," New J. Phys. **6**, 177 (2004).
23. Y. Mao, X. Tong, Z. Wang, L. Zhan, P. Hu, and L. Chen, "Wavelength-tunable 10 GHz actively harmonic mode-locked fiber laser based on semiconductor optical amplifier," Appl. Phys. B **121**, 517 (2015).
24. A. J. Mercante, S. Shi, P. Yao, L. Xie, R. M. Weikle, and D. W. Prather, "Thin film lithium niobate electro-optic modulator with terahertz operating bandwidth," Opt. Express **26**, 14810 (2018).
25. J. Qin, R. Dai, Y. Li, Y. Meng, Y. Xu, S. Zhu, and F. Wang, "20 GHz actively mode-locked thulium fiber laser," Opt. Express **26**, 25769 (2018).
26. W. H. Glenn, M. J. Brienza, and A. J. DeMaria, "Mode locking of an organic dye laser," Appl. Phys. Lett. **12**, 54 (1968).
27. C. V. Shank and E. P. Ippen, "Subpicosecond kilowatt pulses from a mode-locked cw dye laser," Appl. Phys. Lett. **24**, 373 (1974).
28. C. Ausschnitt, R. Jain, and J. Heritage, "Cavity length detuning characteristics of the synchronously mode-locked CW dye laser," IEEE J. Quantum Elect. **15**, 912 (1979).
29. S. Vasilyev, M. Mirov, and V. Gapontsev, "Kerr-lens mode-locked femtosecond polycrystalline Cr^{2+}: ZnS and Cr^{2+}: ZnSe lasers," Opt. Express **22**, 5118 (2014).
30. Z.-Y. Gao, J.-F. Zhu, K. Wang, J.-L. Wang, Z.-H. Wang, and Z.-Y. Wei, "Diode-pumped Kerr-lens mode-locked femtosecond Yb:YAG ceramic laser," Chin. Phys. B **25**, 024205 (2016).
31. S. Ghanbari, R. Akbari, and A. Major, "Femtosecond Kerr-lens mode-locked alexandrite laser," Opt. Express **24**, 14836 (2016).
32. U. Keller, K. J. Weingarten, F. X. Kartner, D. Kopf, B. Braun, I. D. Jung, R. Fluck, C. Honninger, N. Matuschek, and J. Aus der Au, "Semiconductor saturable absorber mirrors (SESAM's) for femtosecond to nanosecond pulse generation in solid-state lasers," IEEE J. Quantum Electron. **2**, 435 (1996).
33. F. Wang, A. Rozhin, V. Scardaci, Z. Sun, F. Hennrich, I. H. White, W. I. Milne, and A. C. Ferrari, "Wideband-tuneable, nanotube mode-locked, fibre laser," Nat. Nanotechnol. **3**, 738 (2008).
34. G. Sobon, "Mode-locking of fiber lasers using novel two-dimensional nanomaterials: graphene and topological insulators [Invited]," Photon. Res. **3**, A56 (2015).
35. T. Hasan, Z. Sun, F. Wang, F. Bonaccorso, P. H. Tan, A. G. Rozhin, and A. C. Ferrari, "Nanotube–polymer composites for ultrafast photonics," Adv. Mater. **21**, 3874 (2009).
36. A. Martinez and Z. Sun, "Nanotube and graphene saturable absorbers for fibre lasers," Nature Photon. **7**, 842 (2013).
37. G. Wang, A. A. Baker-Murray, and W. J. Blau, "Saturable absorption in 2D nanomaterials and related photonic devices," Laser Photon. Rev. **13**, 1800282 (2019).
38. B. Guo, Q. Xiao, S. Wang, and H. Zhang, "2D layered materials: synthesis, nonlinear optical properties, and device applications," Laser Photon. Rev. **13**, 1800327 (2019).
39. U. Keller, W. H. Knox, and H. Roskos, "Coupled-cavity resonant passive mode-locked (RPM) Ti:sapphire laser," Opt. Lett. **15**, 1377 (1990).

40. I. D. Jung, F. X. Kärtner, N. Matuschek, D. H. Sutter, F. Morier-Genoud, G. Zhang, U. Keller, V. Scheuer, M. Tilsch, and T. Tschudi, "Self-starting 6.5-fs pulses from a Ti:sapphire laser," Opt. Lett. **22**, 1009 (1997).
41. F. X. Kurtner, J. A. der Au, and U. Keller, "Mode-locking with slow and fast saturable absorbers – what's the difference?" IEEE J. Sel. Top. Quantum Electron, **4**, 159 (1998).
42. R. Paschotta and U. Keller, "Passive mode-locking with slow saturable absorbers," Appl. Phys. B **73**, 653 (2001).
43. G. J. Spühler, K.J. Weingarten, R. Grange, L. Krainer, M. Halml, V. Liverini, M. Golling, S. Schon, and U. Keller, "Semiconductor saturable absorber mirror structures with low saturation fluence," Appl. Phys. B **81**, 27 (2005).
44. C. Hönninger, R. Paschotta, F. Morier-Genoud, M. Moser, and U. Keller, "*Q*-switching stability limits of continuous-wave passive mode locking," J. Opt. Soc. Am. B **16**, 46 (1999).
45. S. A. Campbell, *The Science and Engineering of Microelectronic Fabrication* (Oxford University, 2001).
46. E. U. Rafailov, A. A. Lagatsky, S. A. Zolotovskaya, and W. Sibbett, "Compact and efficient mode-locked lasers based on QD-SESAMs," Proc. SPIE **6998**, 69980B (2008).
47. S. Iijima, "Synthesis of carbon nanotubes," Nature **354**, 56 (1991).
48. H.-S. P. Wong and D. Akinwande, *Carbon Nanotube and Graphene Device Physics* (Cambridge University, 2011).
49. J. W. G. Wilder, L. C. Venema, A. G. Rinzler, R. E. Smalley, and C. Dekker, Electronic structure of atomically resolved carbon nanotubes, Nature **391**, 59 (1998).
50. S. Reich, M. Dworzak, A. Hoffmann, C. Thomsen, and M. S. Strano, "Excited-state carrier lifetime in single-walled carbon nanotubes," Phys. Rev. B **71**, 033402 (2005).
51. Y.-Z. Ma, J. Stenger, J. Zimmermann, S. M. Bachilo, R. E. Smalley, R. B. Weisman, and G. R. Fleming, "Ultrafast carrier dynamics in single-walled carbon nanotubes probed by femtosecond spectroscopy," J. Chem. Phys. **120**, 3368 (2004).
52. S. Set, H. Yaguchi, M. Jablonski, Y. Tanaka, Y. Sakakibara, A. Rozhin, M. Tokumoto, H. Kataura, and Y. Achiba "A noise suppressing saturable absorber at 1550 nm based on carbon nanotube technology," in *Optical Fiber Communications Conference* (2003), p. 723.
53. S. Kivistö, T. Hakulinen, A. Kaskela, B. Aitchison, D. P. Brown, A. G. Nasibulin, E. I. Kauppinen, A. Härkönen, and O. Okhotnikov, "Carbon nanotube films for ultrafast broadband technology," Opt. Express **17**, 2358 (2009).
54. M. A. Solodyankin, E. D. Obraztsova, A. S. Lobach, A. I. Chernov, A. V. Tausenev, V. Konov, I, and E. M. Dianov, "Mode-locked 1.93 μm thulium fiber laser with a carbon nanotube absorber," Opt. Lett. **33**, 1336 (2008).
55. L. Huang, Y. Zhang, and X. Liu, "Dynamics of carbon nanotube-based mode-locking fiber lasers," Nanophotonics **9**, 2731 (2020).
56. C. Wei, Y. Lyu, H. Shi, Z. Kang, H. Zhang, G. Qin, and Y. Liu, "Mid-infrared *Q*-switched and mode-locked fiber lasers at 2.87 μm based on carbon nanotube," IEEE J Quantum Electron. **25**, 1100206 (2019).
57. R. R. Nair, P. Blake, A. N. Grigorenko, K. S. Novoselov, T. J. Booth, T. Stauber, N. M. R. Peres, and A. K. Geim, "Fine structure constant defines visual transparency of graphene," Science **320**, 1308 (2008).
58. Z. Sun, T. Hasan, F. Torrisi, D. Popa, G. Privitera, F. Wang, F. Bonaccorso, D. M. Basko, and A. C. Ferrari, "Graphene mode-locked ultrafast laser," ACS Nano **4**, 803 (2010).
59. G. Sobon, J. Sotor, I. Pasternak, A. Krajewska, W. Strupinski, and K. M. Abramski, "Multilayer graphene-based saturable absorbers with scalable modulation depth for mode-locked Er- and Tm-doped fiber lasers," Opt. Mater. Express **5**, 2884 (2015).
60. K. Seibert, G. C. Cho, W. Kütt, H. Kurz, D. H. Reitze, J. I. Dadap, H. Ahn, M. C. Downer, and A. M. Malvezzi, "Femtosecond carrier dynamics in graphite," Phys. Rev. B **42**, 2842 (1990).
61. M. Breusing, C. Ropers, and T. Elsaesser, "Ultrafast carrier dynamics in graphite," Phys. Rev. Lett. **102**, 086809 (2009).
62. Q. Bao, H. Zhang, Y. Wang, Z. Ni, Y. Yan, Z. X. Shen, K. P. Loh, and D. Y. Tang, "Atomic-layer graphene as a saturable absorber for ultrafast pulsed lasers," Adv. Funct. Mater **19**, 3077 (2009).
63. K. S. Novoselov, A. K. Geim, S. V. Morozov, D. Jiang, Y. Zhang, S. V. Dubonos, I. V. Grigorieva, and A. A. Firsov, "Electric field effect in atomically thin carbon films," Science **306**, 666 (2004).
64. I. H. Baek, H. W. Lee, S. Bae, B. H. Hong, Y. H. Ahn, D.-I. Yeom, and F. Rotermund, "Mode-locking of sub-70-fs Ti:sapphire laser by graphene saturable absorber," Appl. Phys. Express **5**, 032701 (2013).
65. H. Zhang, D. Y. Tang, L. M. Zhao, Q. L. Bao, and K. P. Loh, "Large energy mode locking of an erbium-doped fiber laser with atomic layer graphene," Opt. Express **17**, 17630 (2009).
66. D. I. M. Zen, N. Saidin, S. S. A. Damanhuri, S. W. Harun, H. Ahmad, M. A. Ismail, K. Dimyati, A. Halder, M. C. Paul, S. Das, M. Pal, and S. K. Bhadra, "Mode-locked thulium bismuth codoped fiber laser using graphene saturable absorber in ring cavity: reply," Appl. Opt. **52**, 1226 (2013).
67. G. Zhu, X. Zhu, K. Balakrishnan, R. A. Norwood, and N. Peyghambarian, "Fe^{2+}: ZnSe and graphene *Q*-switched singly Ho^{3+}-doped ZBLAN fiber lasers at 3 μm," Opt. Mater. Express **3**, 1365 (2013).
68. A. Malouf, O. Henderson-Sapir, S. Set, S. Yamashita, and D. J. Ottaway, "Two-photon absorption and saturable absorption of mid-IR in graphene," Appl. Phys. Lett. **114**, 091111 (2019).
69. M. Xu, T. Liang, M. Shi, and H. Chen, "Graphene-like two-dimensional materials," Chem. Rev. **113**, 3766 (2013).
70. R. I. Woodward, E. J. R. Kelleher, R. C. T. Howe, G. Hu, F. Torrisi, T. Hasan, S. V. Popov, and J. R. Taylor, "Tunable *Q*-switched fiber laser based on saturable edge-state absorption in few-layer molybdenum disulfide (MoS_2)," Opt. Express **22**, 31113 (2014).
71. K. F. Mak, C. Lee, J. Hone, J. Shan, and T. F. Heinz, "Atomically thin MoS_2: a new direct-gap semiconductor," Phys. Rev. Lett. **105**, 136805 (2010).
72. A. Kuc, N. Zibouche, and T. Heine, "Influence of quantum confinement on the electronic structure of the transition metal sulfide TS_2," Phys. Rev. B **83**, 245213 (2011).
73. W. S. Yun, S. W. Han, S. C. Hong, I. G. Kim, and J. D. Lee, "Thickness and strain effects on electronic structures of transition metal dichalcogenides: 2H-MX_2 semiconductors (M = Mo, W; X = S, Se, Te)," Phys. Rev. B **85**, 033305 (2012).
74. G. J. Spühler, K. J. Weingarten, R. Grange, L. Krainer, M. Haiml, V. Liverini, M. Golling, S. Schön, and U. Keller, "Semiconductor saturable absorber mirror structures with low saturation fluence," Appl. Phys. B **81**, 27 (2005).
75. D. J. H. C. Maas, A.-R. Bellancourt, M. Hoffmann, B. Rudin, Y. Barbarin, M. Golling, T. Südmeyer, and U. Keller, "Growth parameter optimization for fast quantum dot SESAMs," Opt. Express **16**, 18646 (2008).
76. B. W. Tilma, M. Mangold, C. A. Zaugg, S. M. Link, D. Waldburger, A. Klenner, A. S. Mayer, E. Gini, M. Golling, and U. Keller, "Recent advances in ultrafast semiconductor disk lasers," Light: Sci. Appl. **4**, e310 (2015).
77. F. Saltarelli, A. Diebold, I. J. Graumann, C. R. Phillips, and U. Keller, "Self-phase modulation cancellation in a high-power ultrafast thin-disk laser oscillator," Optica **5**, 1603 (2018).
78. M. Mangold, V. J. Wittwer, C. A. Zaugg, S. M. Link, M. Golling, B. W. Tilma, and U. Keller, "Femtosecond pulses from a modelocked integrated external-cavity surface emitting laser (MIXSEL)," Opt. Express **21**, 24904 (2013).
79. X. Wang, Y. J. Zhu, C. Jiang, Y. X. Guo, X. T. Ge, H. M. Chen, J. Q. Ning, C. C. Zheng, Y. Peng, X. H. Li, and Z. Y. Zhang, "InAs/GaAs quantum dot semiconductor saturable absorber for controllable dual-wavelength passively *Q*-switched fiber laser," Opt. Express **27**, 20649 (2019).
80. T. Finke, J. Nürnberg, V. Sichkovskyi, M. Golling, U. Keller, and J. P. Reithmaier, "Temperature resistant fast $In_xGa_{1-x}As$/GaAs quantum dot saturable absorber for the epitaxial integration into semiconductor surface emitting lasers," Opt. Express **28**, 20954 (2020).
81. S.-H. Kwona, D. H. Song, I.-S. Kim, and D.-K. Ko, "Operating characteristics of a SESAM-assisted mode-locked laser oscillator with the location of the SESAM position," Opt. Laser. Technol. **133**, 106560 (2021).
82. A. E. H. Oehler, T. Südmeyer, K. J. Weingarten, and U. Keller, "100 GHz passively mode-locked Er:Yb:glass laser at 1.5 μm with 1.6-ps pulses," Opt. Express **16**, 21930 (2008).
83. U. Keller, "Ultrafast solid-state laser oscillators: a success story for the last 20 years with no end in sight," Appl. Phys. B **100**, 15 (2010).
84. C. J. Saraceno, F. Emaury, C. Schriber, M. Hoffmann, M. Golling, T. Südmeyer, and U. Keller, "Ultrafast thin-disk laser with 80 μJ pulse energy and 242 W of average power," Opt. Lett. **39**, 9 (2014).
85. F. Saltarelli, I. J. Graumann, L. Lang, D. Bauer, C. R. Phillips, and U. Keller, "Power scaling of ultrafast oscillators: 350-W average-power sub-picosecond thin-disk laser," Opt. Express **27**, 31465 (2019).

86. K. A. Williams, M. G. Thompson, and I. H. White, "Long-wavelength monolithic mode-locked diode lasers," New J. Phys. **6**, 179 (2004).
87. E. A. Avrutin, J. H. Marsh, and E. L. Portnoi, "Monolithic and multi-gigahertz mode-locked semiconductor lasers: constructions, experiments, models and applications," IEEE Proc. Optoelectron. **147**, 251 (2000).
88. U. Keller and A. C. Tropper, "Passively modelocked surface-emitting semiconductor lasers," Phys. Rep. **429**, 67 (2006).
89. C. G. E. Alfieri, D. Waldburger, M. Golling, and U. Keller, "High-power sub-300-femtosecond quantum dot semiconductor disk lasers," IEEE Photon. Technol. Lett. **30**, 525 (2018).
90. A. Laurain, I. Kilen, J. Hader, A. R. Perez, P. Ludewig, W. Stolz, S. Addamane, G. Balakrishnan, S. W. Koch, and J. V. Moloney, "Modeling and experimental realization of modelocked VECSEL producing high power sub-100 fs pulses," Appl. Phys. Lett. **113**, 121113 (2018).
91. M. Scheller, T. L. Wang, B. Kunert, W. Stolz, S. W. Koch, and J. V. Moloney, "Passively mode locked VECSEL emitting 682 fs pulses with 5.1 W of average output power," Electron Lett. **48**, 588 (2012).
92. D. Lorenser, D. J. H. C. Maas, H. J. Unold, A-R. Bellancourt, B. Rudi, E. Gini, D. Ebling, and U. Keller, "50-GHz passively mode-locked surface-emitting semiconductor laser with 100 mW average output power," IEEE J. Quantum Electron. **42**, 838 (2006).
93. K. G. Wilcox, A. C. Tropper, H. E. Beere, D. A. Ritchie, B. Kunert, B. Heinen, and W. Stolz, "4.35 kW peak power femtosecond pulse mode-locked VECSEL for supercontinuum generation," Opt. Express **21**, 1599 (2013).
94. D. J. H. C. Maas, A-R. Bellancourt, B. Rudin, M. Golling, H. J. Unold, T. Südmeyer, and U. Keller, "Vertical integration of ultrafast semiconductor lasers," Appl. Phys. B **88**, 493 (2007).
95. M. Mangold, C. A. Zaugg, S. M. Link, M. Golling, B. W. Tilma, and U. Keller, "Pulse repetition rate scaling from 5 to 100 GHz with a high-power semiconductor disk laser," Opt. Express **22**, 6099 (2014).
96. B. Rudin, V. J. Wittwer, D. J. H. C. Maas, M. Hoffmann, O. D. Sieber, Y. Barbarin, M. Golling, T. Südmeyer, and U. Keller, "High-power MIXSEL: an integrated ultrafast semiconductor laser with 6.4 W average power," Opt. Express **18**, 27582 (2010).
97. C. G. E. Alfieri, D. Waldburger, J. Nürnberg, M. Golling, and U. Keller, "Sub-150-fs pulses from an optically pumped broadband mode locked integrated external-cavity surface emitting laser," Opt. Lett. **44**, 25 (2019).
98. F. Labaye, M. Gaponenko, V. J. Wittwer, A. Diebold, C. Paradis, N. Modsching, L. Merceron, F. Emaury, I. J. Graumann, C. R. Phillips, C. J. Saraceno, C. Kränkel, U. Keller, and T. Südmeyer, "Extreme ultraviolet light source at a megahertz repetition rate based on high-harmonic generation inside a mode-locked thin-disk laser oscillator," Opt. Lett. **42**, 5170 (2017).
99. A. A. Lagatsky, F. Fusari, S. Calvez, S. V. Kurilchik, V. E. Kisel, N. V. Kuleshov, M. D. Dawson, C. T. A. Brown, and W. Sibbett, "Femtosecond pulse operation of a Tm,Ho-codoped crystalline laser near 2 μm," Opt. Lett. **35**, 172 (2010).
100. V. Aleksandrov, A. Gluth, V. Petrov, I. Buchvarov, G. Steinmeyer, J. Paajaste, S. Suomalainen, A. Härkönen, M. Guina, X. Mateos, F. Díaz, and U. Griebner, "Mode-locked Tm,Ho:KLu$(WO_4)_2$ laser at 2060 nm using InGaSb-based SESAMs," Opt. Express **23**, 4614 (2015).
101. K. Merghem, R. Teissier, G. Aubin, A. M. Monakhov, A. Ramdane, and A. N. Baranov, "Passive mode locking of a GaSb-based quantum well diode laser emitting at 2.1 μm," Appl. Phys. Lett. **107**, 111109 (2015).
102. P. Holl, M. Rattunde, S. Adler, S. Kaspar, W. Bronner, A. Bachle, R. Aidam, and J. Wagner, "Recent advances in power scaling of GaSb-based semiconductor disk lasers," IEEE J. Sel. Top. Quantum Electron. **21**, 324 (2015).
103. Y. Zhao, Y. Wang, X. Zhang, X. Mateos, Z. Pan, P. Loiko, W. Zhou, X. Xu, J. Xu, D. Shen, S. Suomalainen, A. Härkönen, M. Guina, U. Griebner, and V. Petrov, "87 fs mode-locked Tm,Ho:$CaYAlO_4$ laser at ~2043 nm," Opt. Lett. **43**, 915 (2018).
104. P. W. Metz, F. Reichert, F. Moglia, S. Müller, D.-T. Marzahl, C. Kränkel, and G. Huber, "High-power red, orange, and green Pr^{3+}:$LiYF_4$ lasers," Opt. Lett. **39**, 3193 (2014).
105. K. Gürel, V. J. Wittwer, M. Hoffmann, C. J. Saraceno, S. Hakobyan, B. Resan, A. Rohrbacher, K. Weingarten, S. Schilt, and T. Südmeyer, "Green-diode-pumped femtosecond Ti:sapphire laser with up to 450 mW average power," Opt. Express **23**, 30043 (2015).
106. Y. Zhang, V. Petrov, U. Griebner, X. Zhang, H. Yu, H. Zhang, and J. Liu, "Diode-pumped SESAM mode-locked Yb:CLNGG laser," Opt. Laser Technol. **69**, 144 (2015).
107. J. Ma, Z. Pan, J. Wang, H. Yuan, H. Cai, G. Xie, L. Qian, D. Shen, and D. Tang, "Generation of sub-50fs soliton pulses from a mode-locked Yb, Na:CNGG disordered crystal laser," Opt. Express **25**, 14968 (2017).
108. A. S. Mayer, C. R. Phillips, and U. Keller, "Watt-level 10-gigahertz solid-state laser enabled by self-defocusing nonlinearities in an aperiodically poled crystal," Nat. Commun. **8**, 1673 (2017).
109. R. Akbari, K. A. Fedorova, E. U. Rafailov, and A. Major, "Diode-pumped ultrafast Yb:KGW laser with 56 fs pulses and multi-100 kW peak power based on SESAM and Kerr-lens mode locking," Appl. Phys. B **123**, 123 (2017).
110. R. Grange, S. Zeller, M. Haiml, O. Ostinelli, E. Gini, S. Schon, and U. Keller, "Antimonide semiconductor saturable absorber for passive mode locking of a 1.5-μm Er:Yb:glass laser at 10 GHz," IEEE Photon. Technol. Lett. **18**, 805 (2006).
111. A. Choudhary, A. A. Lagatsky, Z. Y. Zhang, K. J. Zhou, Q. Wang, R. A. Hogg, K. Pradeesh, E. U. Rafailov, W. Sibbett, C. T. A. Brown, and D. P. Shepherd, "A diode-pumped 1.5 μm waveguide laser mode-locked at 6.8 GHz by a quantum dot SESAM," Laser Phys. Lett. **10**, 105803 (2013).
112. N. K. Stevenson, C. T. A. Brown, J.-M. Hopkins, M. D. Dawson, C. Kränkel, and A. A. Lagatsky, "Diode-pumped femtosecond Tm^{3+}-doped $LuScO_3$ laser near 2.1 μm," Opt. Lett. **43**, 1287 (2018).
113. X. Bu, Y. Shi, J. Xu, H. Li, and P. Wang, "408-fs SESAM mode locked Cr:ZnSe laser," Proc. SPIE **10619**, 1061903 (2018).
114. Y. Wang, W. Jing, P. Loiko, Y. Zhao, H. Huang, X. Mateos, S. Suomalainen, A. Härkönen, M. Guina, U. Griebner, and V. Petrov, "Sub-10 optical-cycle passively mode-locked Tm:$(Lu_{2/3}Sc_{1/3})_2O_3$ ceramic laser at 2 μm," Opt. Express **26**, 10299 (2018).
115. Y. Wang, Y. Zhao, Z. Pan, S. Suomalainen, A. Härkönen, M. Guina, U. Griebner, L. Wang, P. Loiko, X. Mateos, W. Chen, and V. Petrov, "73-fs SESAM mode-locked Tm,Ho:CNGG laser at 2061 nm," Proc. SPIE **11259**, 1125929 (2020).
116. E. Sorokin and I. T. Sorokina, "Femtosecond operation and random quasi-phase-matched self-doubling of ceramic Cr:ZnSe laser," in *CLEO* (2010), paper CTuGG2.
117. E. Sorokin, N. Tolstik, K. I. Schaffers, and I. T. Sorokina, "Femtosecond SESAM-mode locked Cr:ZnS laser," Opt. Express **20**, 28947 (2012).
118. I. J. Graumann, A. Diebold, C. G. E. Alfieri, F. Emaury, B. Deppe, M. Golling, D. Bauer, D. Sutter, C. Kränkel, C. J. Saraceno, C. R. Phillips, and U. Keller, "Peak-power scaling of femtosecond Yb:Lu_2O_3 thin-disk lasers," Opt. Express **25**, 22519 (2017).
119. F. Saltarelli, A. Diebold, I. J. Graumann, C. R. Phillips, and U. Keller, "Self-phase modulation cancellation in a high-power ultrafast thin-disk laser oscillator," Opt. Lett. **5**, 25 (2018).
120. A. Härkönen, S. Suomalainen, A. Rantamäki, J. Nikkinen, Y. Wang, U. Griebner, G. Steinmeyer, and M. Guina, "1.34 μm VECSEL mode-locked with a GaSb-based SESAM," Opt. Lett. **43**, 3353 (2018).
121. T. R. Schibli, K. Minoshima, H. Kataura, E. Itoga, N. Minami, S. Kazaoui, K. Miyashita, M. Tokumoto, and Y. Sakakibara, "Ultrashort pulse-generation by saturable absorber mirrors based on polymer-embedded carbon nanotubes," Opt. Express **13**, 8025 (2005).
122. D. V. Khudyakov, A. S. Lobach, and V. A. Nadtochenko, "Passive mode locking in a Ti:sapphire laser using a single-walled carbon nanotube saturable absorber at a wavelength of 810 nm," Opt. Lett. **35**, 2675 (2010).
123. I. H. Baek, S. Y. Choi, H. W. Lee, W. B. Cho, V. Petrov, A. Agnesi, V. Pasiskevicius, D. Yeom, K. Kim, and F. Rotermund, "Single-walled carbon nanotube saturable absorber assisted high-power mode-locking of a Ti:sapphire laser," Opt. Express **19**, 7833 (2011).
124. A. Schmidt, S. Rivier, G. Steinmeyer, J. H. Yim, W. B. Cho, S. Lee, F. Rotermund, M. C. Pujol, X. Mateos, M. Aguiló, F. Díaz, V. Petrov, and U. Griebner, "Passive mode locking of Yb:KLuW using a single-walled carbon nanotube saturable absorber," Opt. Lett. **33**, 729 (2008).
125. S. Y. Choi, T. Calmano, F. Rotermund, and C. Kränkel, "2-GHz carbon nanotube mode-locked Yb:YAG channel waveguide laser," Opt. Express **26**, 5140 (2018).
126. W. B. Cho, J. H. Yim, S. Y. Choi, S. Lee, U. Griebner, V. Petrov, and F. Rotermund, "Mode-locked self-starting Cr:forsterite laser using a single-walled carbon nanotube saturable absorber," Opt. Lett. **33**, 2449 (2008).

127. Z. Pan, Y. Wang, Y. Zhao, H. Yuan, X. Dai, H. Cai, J. E. Bae, S. Y. Choi, F. Rotermund, X. Mateos, J. M. Serres, P. Loiko, U. Griebner, and V. Petrov, "Generation of 84-fs pulses from a mode-locked Tm:CNNGG disordered garnet crystal laser," Photon. Res. **6**, 800 (2018).
128. N. Tolstik, O. Okhotnikov, E. Sorokin, and I. T. Sorokina, "Femtosecond Cr:ZnS laser at 2.35 μm mode-locked by carbon nanotubes," Proc. SPIE **8959**, 89591A (2014).
129. W. B. Cho, A. Schmidt, J. H. Yim, S. Y. Choi, S. Lee, F. Rotermund, U. Griebner, G. Steinmeyer, V. Petrov, X. Mateos, M. C. Pujol, J. J. Carvajal, M. Aguiló, and F. Díaz, "Passive mode-locking of a Tm-doped bulk laser near 2 μm using a carbon nanotube saturable absorber," Opt. Express **17**, 11007 (2009).
130. J. Ma, G. Xie, P. Lv, W. Gao, P. Yuan, L. Qian, U. Griebner, V. Petrov, H. Yu, H. Zhang, and J. Wang, "Wavelength-versatile graphene-gold film saturable absorber mirror for ultra-broadband mode-locking of bulk lasers," Sci. Rep. **4**, 5016 (2014).
131. A. G. Khrimchuk and P. A. Obraztsov, "11-GHz waveguide Nd:YAG laser CW mode-locked with single-layer graphene," Sci. Rep. **5**, 11172 (2015).
132. N. Tolstik, E. Sorokin, and I. T. Sorokina, "Graphene mode-locked Cr:ZnS laser with 41 fs pulse duration," Opt. Express **22**, 5564 (2014).
133. C. Feng, X. Zhang, J. Wang, Z. Liu, Z. Cong, H. Rao, Q. Wang, and J. Fang, "Passively mode-locked Nd^{3+}:YVO_4 laser using a molybdenum disulfide as saturable absorber," Opt. Mater. Express **6**, 1358 (2016).
134. L. Tao, X. Huang, J. He, Y. Lou, L. Zeng, Y. Li, H. Long, J. Li, L. Zhang, and Y. H. Tsang, "Vertically standing $PtSe_2$ film: a saturable absorber for a passively mode-locked Nd:$LuVO_4$ laser," Photon. Res. **6**, 750 (2018).
135. K. Seger, N. Meiser, S. Y. Choi, B. H. Jung, D.-I. Yeom, F. Rotermund, O. Okhotnikov, F. Laurell, and V. Pasiskevicius, "Carbon nanotube mode-locked optically-pumped semiconductor disk laser," Opt. Express **21**, 17806 (2013).
136. C. A. Zaugg, Z. Sun, V. J. Wittwer, D. Popa, S. Milana, T. S. Kulmala, R. S. Sundaram, M. Mangold, O. D. Sieber, M. Golling, Y. Lee, J. H. Ahn, A. C. Ferrari, and U. Keller, "Ultrafast and widely tuneable vertical-external-cavity surface-emitting laser, mode-locked by a graphene-integrated distributed Bragg reflector," Opt. Express, **21**, 31548 (2013).
137. S. Husaini and R. G. Bedford, "Graphene saturable absorber for high power semiconductor disk laser mode-locking," Appl. Phys. Lett. **104**, 161107 (2014).
138. M. S. Gaponenko, V. E. Kisel, N. V. Kuleshov, A. M. Malyarevich, K. V. Yumashev, and A. A. Onushchenko, "Compact passively *Q*-switched diode-pumped Tm:$KY(WO_4)_2$ laser with 8 ns/30 μJ pulses," Laser Phys. Lett. **7**, 286 (2010).
139. M. Zhang, R. C. T. Howe, R. I. Edmund, J. R. Kelleher, F. Torrisi, G. Hu, S. V. Popov, J. R. Taylor, and T. Hasan, "Solution processed MoS_2-PVA composite for sub-bandgap mode-locking of a wideband tunable ultrafast Er:fiber laser," Nano Res. **8**, 1522 (2015).
140. M. Yi and Z. Shen, "A review on mechanical exfoliation for the scalable production of graphene," J. Mater. Chem. A **3**, 11700 (2015).
141. H. Zhang, S. B. Lu, J. Zheng, J. Du, S. C. Wen, D. Y. Tang, and K. P. Loh, "Molybdenum disulfide (MoS_2) as a broadband saturable absorber for ultra-fast photonics," Opt. Express **22**, 7249 (2014).
142. D. Steinberg, R. M. Gerosa, F. N. Pellicer, J. D. Zapata, S. H. Domingues, E. A. Thoroh de Souza, and L. A. M. Saito, "Graphene oxide and reduced graphene oxide as saturable absorbers onto D-shaped fibers for sub 200-fs EDFL mode-locking," Opt. Mater. Express **8**, 144 (2018).
143. J. N. Coleman, M. Lotya, A. O'Neill, S. D. Bergin, P. J. King, U. Khan, and V. Nicolosi, "Two-dimensional nanosheets produced by liquid exfoliation of layered materials," Science **331**, 568 (2011).
144. T. Jiang, K. Yin, C. Wang, J. You, H. Ouyang, R. Miao, C. Zhang, K. Wei, H. Li, H. Chen, R. Zhang, X. Zheng, Z. Xu, X. Cheng, and H. Zhang, "Ultrafast fiber lasers mode-locked by two-dimensional materials: review and prospect," Photon. Res. **8**, 78 (2020).
145. D. Popa, Z. Sun, T. Hasan, W. B. Cho, F. Wang, F. Torrisi, and A. C. Ferrari, "74-fs nanotube-mode-locked fiber laser," Appl. Phys. Lett. **101**, 153107 (2012).
146. D. Mao, B. Jiang, W. Zhang, and J. Zhao, "Pulse-state switchable fiber laser mode-locked by carbon nanotubes," IEEE Photon. Technol. Lett. **27**, 253 (2015).
147. Y. Meng, Y. Li, Y. Xu, and F. Wang, "Carbon nanotube mode-locked thulium fiber laser with 200 nm tuning range," Sci. Rep. **7**, 45109 (2017).
148. J. W. Nicholson, R. S. Windeler, and D. J. DiGiovanni, "Optically driven deposition of single-walled carbon-nanotube saturable absorbers on optical fiber end-faces," Opt. Express **15**, 9176 (2007).
149. G. Sobon, A. Duzynska, M. Świniarski, J. Judek, J. Sotor, and M. Zdrojek, "CNT-based saturable absorbers with scalable modulation depth for thulium-doped fiber lasers operating at 1.9 μm," Sci. Rep. **7**, 45491 (2017).
150. W. Liu, M. Liu, X. Chen, T. Shen, M. Lei, J. Guo, H. Deng, W. Zhang, C. Dai, X. Zhang, and Z. Wei, "Ultrafast photonics of two dimensional $AuTe_2Se_{4/3}$ in fiber lasers," Commun. Phys. **3**, 15 (2020).
151. K. Kieu and M. Mansuripur, "Femtosecond laser pulse generation with a fiber taper embedded in carbon nanotube/polymer composite," Opt. Lett. **32**, 2242 (2007).
152. Y.-W. Song, S. Yamashita, and S. Maruyama, "Single-walled carbon nanotubes for high-energy optical pulse formation," Appl. Phys. Lett. **92**, 021115 (2008).
153. M. Liu, X.-W. Zheng, Y.-L. Qi, H. Liu, A.-P. Luo, Z.-C. Luo, W.-C. Xu, C.-J. Zhao, and H. Zhang, "Microfiber-based few-layer MoS_2 saturable absorber for 2.5 GHz passively harmonic mode-locked fiber laser," Opt. Express **22**, 22841 (2014).
154. M. Zhang, J. Li, H. Chen, J. Zhang, J. Yin, T. He, J. Wang, M. Zhang, B. Zhang, J. Yuan, P. Yan, and S. Ruan, "Group IIIA/IVA monochalcogenides nanosheets for ultrafast photonics," APL Photon. **4**, 090801 (2019).
155. J. D. Yin, F. X. Zhu, J. T. Lai, H. Chen, M. Y. Zhang, J. Q. Zhang, J. T. Wang, T. C. He, B. Zhang, J. P. Yuan, P. G. Yan, and S. C. Ruan, "Hafnium sulfide nanosheets for ultrafast photonic device," Adv. Opt. Mater. **7**, 1801303 (2018).
156. X. Wu, Z. W. Zhou, J. D. Yin, M. Zhang, L. L. Zhou, Q. X. Na, J. T. Wang, Y. Yu, J. B. Yang, and R. H. Chi, "Ultrafast fiber laser based on $HfSe_2$ saturable absorber," Nanotechonlogy **31**, 24 (2020).
157. X. Xu, M. He, C. Quan, R. Wang, C. Liu, Q. Zhao, Y. Zhou, J. Bai, and X. Xu, "Saturable absorption properties of ReS_2 films and mode-locking application based on double-covered ReS_2 micro fiber," J. Lightwave Technol. **36**, 5130 (2018).
158. G. Hu, L. Yang, Z. Yang, Y. Wang, X. Jin, J. Dai, Q. Wu, S. Liu, X. Zhu, X. Wang, T. Wu, R. C. T. Howe, T. Albrow-Owen, L. W. T. Ng, Q. Yang, L. G. Occhipinti, R. I. Woodward, E. J. R. Kelleher, Z. Sun, X. Huang, M. Zhang, C. D. Bain, and T. Hasan, "A general ink formulation of 2D crystals for wafer-scale inkjet printing," Sci. Adv. **6**, eaba5029 (2020).
159. Y. Gao, W. Shi, W. Wang, Y. Leng, and Y. Zhao, "Inkjet printing patterns of highly conductive pristine graphene on flexible substrates," Ind. Eng. Chem. Res. **53**, 16777 (2014).
160. Y. I. Jhon, J. Koo, B. Anasori, M. Seo, J. Lee, Y. Gogotsi, and Y. M. Jhon, "2D materials: metallic MXene saturable absorber for femtosecond mode-locked lasers," Adv Mater. **29**, 1702496 (2017).
161. G. Hu, T. A. Owen, X. Jin, A. Ali, Y. Hu, R. C. T. Howe, K. Shehzad, Z. Yang, X. Zhu, R. I. Woodward, T.-C. Wu, H. Jussila, J.-B. Wu, P. Peng, P.-H. Tan, Z. Sun, E. J. R. Kelleher, M. Zhang, Y. Xu, and T. Hasan, "Black phosphorus ink formulation for inkjet printing of optoelectronics and photonics," Nat. Commun. **8**, 1 (2017).
162. X. Jin, G. Hu, M. Zhang, Y. Hu, T. A. Owen, R. C. T. Howe, T.-C. Wu, Q. Wu, Z. Zheng, and T. Hasan, "102 fs pulse generation from a long-term stable, inkjet-printed black phosphorus-mode-locked fiber laser," Opt. Express **26**, 12506 (2018).
163. X. Jiang, W. Li, T. Hai, R. Yue, Z. Chen, C. Lao, Y. Ge, G. Xie, Q. Wen, and H. Zhang, "Inkjet-printed MXene micro-scale devices for integrated broadband ultrafast photonics," NPJ 2D Mater. Appl. **3**, 34 (2019).
164. J. Lee, H. Chung, J. Koo, G. Woo, and J. H. Lee, "A 3-D printed saturable absorber for femtosecond mode-locking of a fiber laser," Opt. Mater. **89**, 382 (2019).
165. G. Woo, J. Lee, and J. H. Lee, "A 1.9 μm femtosecond fiber laser using a 3D printed, all-fiberized graphene/polylactic-acid saturable absorber," Laser Phys. Lett **16**, 085101 (2019).
166. K. Kieu and F. W. Wise, "All-fiber normal-dispersion femtosecond laser," Opt. Express **16**, 11453 (2008).
167. L. Hou, H. Guo, Y. Wang, J. Sun, Q. Lin, Y. Bai, and J. Bai, "Sub-200 femtosecond dispersion-managed soliton ytterbium-doped fiber laser based on carbon nanotubes saturable absorber," Opt. Express **26**, 9063 (2018).
168. G. Sobon, A. Duzynska, M. Świniarski, J. Judek, J. Sotor, and M. Zdrojek, "CNT-based saturable absorbers with scalable modulation depth for thulium-doped fiber lasers operating at 1.9 μm," Sci. Rep. **7**, 45491 (2017).

169. Z. Sun, T. Hasan, F. Wang, A. G. Rozhin, I. H. White, and A. C. Ferrari, "Ultrafast stretched-pulse fiber laser mode-locked by carbon nanotubes," Nano Res. **3**, 404 (2010).
170. A. Martinez and S. Yamashita, "Multi-gigahertz repetition rate passively mode locked fiber lasers using carbon nanotubes," Opt. Express **19**, 6155 (2011).
171. J. Wang, X. Liang, G. Hu, Z. Zheng, S. Lin, D. Ouyang, X. Wu, P. Yan, S. Ruan, Z. Sun, and T. Hasan, "152 fs nanotube-mode-locked thulium-doped all-fiber laser," Sci. Rep. **6**, 28885 (2016).
172. Z. Sun, T. Hasan, F. Torrisi, D. Popa, G. Privitera, F. Wang, F. Bonaorso, D. M. Basko, and A. C. Ferrari, "Graphene mode-locked ultrafast laser," ACS Nano **4**, 803 (2010).
173. D. G. Purdie, D. Popa, V. J. Wittwer, Z. Jiang, G. Bonacchini, F. Torrisi, S. Milana, E. Lidorikis, and A. C. Ferrari, "Few-cycle pulses from a graphene mode-locked all-fiber laser," Appl. Phys. Lett. **106**, 253101 (2015).
174. D. Popa, Z. Sun, F. Torrisi, T. Hasan, F. Wang, and A. C. Ferrari, "Sub 200 fs pulse generation from a graphene mode-locked fiber laser," Appl. Phys. Lett. **97**, 203106 (2010).
175. A. Martinez and S. Yamashita, "10 GHz fundamental mode fiber laser using a graphene saturable absorber," Appl. Phys. Lett. **101**, 041118 (2012).
176. Y. Zhang, J. Zhu, P. Li, X. Wang, H. Yu, K. Xiao, C. Li, and G. Zhang, "All-fiber Yb-doped fiber laser passively mode-locking by monolayer MoS_2 saturable absorber," Opt. Commun. **413**, 236 (2018).
177. H. Liu, A.-P. Luo, F.-Z. Wang, R. Tang, M. Liu, Z.-C. Luo, W.-C. Xu, C.-J. Zhao, and H. Zhang, "Femtosecond pulse erbium-doped fiber laser by a few-layer MoS_2 saturable absorber," Opt. Lett. **39**, 4591 (2014).
178. K. Wu, X. Zhang, J. Wang, X. Li, and J. Chen, "WS_2 as a saturable absorber for ultrafast photonic applications of mode-locked and Q-switched lasers," Opt. Express **23**, 11453 (2015).
179. L. Li, Y. Su, Y. Wang, X. Wang, Y. Wang, X. Li, D. Mao, and J. Si, "Femtosecond passively Er-doped mode-locked fiber laser with WS_2 solution saturable absorber," IEEE J. Quantum. Electron. **23**, 44 (2017).
180. R. Khazaeinezhad, S. H. Kassani, H. Jeong, D.-I Yeom, and K. Oh, "Femtosecond soliton pulse generation using evanescent field interaction through tungsten disulfide (WS_2) film," IEEE J. Lightwave Technol. **33**, 3550 (2015).
181. R. Khazaeinezhad, S. H. Kassani, H. Jeong, K. J. Park, B. Yoon Kim, D.-I. Yeom, and K. Oh, "Ultrafast pulsed all-fiber laser based on tapered fiber enclosed by few-layer WS_2 nanosheets," IEEE Photon. Technol. Lett. **27**, 1581 (2015).
182. D. Mao, X. She, B. Du, D. Yang, W. Zhang, K. Song, X. Cui, B. Jiang, T. Peng, and J. Zhao, "Erbium-doped fiber laser passively mode locked with few-layer $WSe_2/MoSe_2$ nanosheets," Sci. Rep. **6**, 23583 (2016).
183. H. Ahmad, S. N. Aidit, N. A. Hassan, M. F. Ismail, and Z. C. Tiu, "Generation of mode-locked erbium-doped fiber laser using $MoSe_2$ as saturable absorber," Opt. Lasers Eng. **55**, 076115 (2016).
184. D. Mao, X. Cui, X. Gan, M. Li, W. Zhang, H. Lu, and J. Zhao, "Passively Q-switched and mode-locked fiber laser based on an ReS_2 saturable absorber," IEEE J. Quantum Electron. **24**, 1100406 (2018).
185. K. Niu, R. Sun, Q. Chen, B. Man, and H. Zhang, "Passively mode-locked Er-doped fiber laser based on SnS_2 nanosheets as a saturable absorber," Photon. Res. **6**, 72 (2018).
186. D. Mao, B. Jiang, X. Gan, C. Ma, Y. Chen, C. Zhao, H. Zhang, J. Zheng, and J. Zhao, "Soliton fiber laser mode locked with two types of film-based Bi_2Te_3 saturable absorbers," Photon. Res. **3**, A43 (2015).
187. H. Liu, X.-W. Zheng, M. Liu, N. Zhao, A.-P. Luo, Z.-C. Luo, W.-C. Xu, H. Zhang, C.-J. Zhao, and S.-C. Wen, "Femtosecond pulse generation from a topological insulator mode-locked fiber laser," Opt. Express **22**, 6868 (2014).
188. L. Jin, X. Ma, H. Zhang, H. Zhang, H. Chen, and Y. Xu, "3 GHz passively harmonic mode-locked Er-doped fiber laser by evanescent field-based nano-sheets topological insulator," Opt. Express **26**, 31244 (2018).
189. B. Guo, S.-H. Wang, Z.-X. Wu, Z.-X. Wang, D.-H. Wang, H. Huang, F. Zhang, Y.-Q. Ge, and H. Zhang, "Sub-200 fs soliton mode-locked fiber laser based on bismuthene saturable absorber", Opt. Express **26**, 22750 (2018).
190. J. Sotor, G. Sobon, W. Macherzynski, P. Paletko, and K. M. Abramski, "Black phosphorus saturable absorber for ultrashort pulse generation," Appl. Phys. Lett. **107**, 051108 (2015).
191. Y. Ge, Z. Zhu, Y. Xu, Y. Chen, S. Chen, Z. Liang, Y. Song, Y. Zou, H. Zeng, S. Xu, H. Zhang, and D. Fan, "Broadband nonlinear photoresponse of 2D TiS_2 for ultrashort pulse generation and all-optical thresholding devices," Adv. Opt. Mater. **6**, 1701166 (2017).
192. P. Yan, R. Lin, S. Ruan, A. Liu, H. Chen, Y. Zheng, S. Chen, C. Guo, and J. Hu, "A practical topological insulator saturable absorber for mode-locked fiber laser," Sci. Rep. **5**, 8690 (2015).
193. P. Yan, R. Lin, S. Ruan, A. Liu, and H. Chen, "A 2.95 GHz, femtosecond passive harmonic mode-locked fiber laser based on evanescent field interaction with topological insulator film," Opt. Express **23**, 154 (2015).
194. J. Boguslawski, G. Sobon, R. Zybala, and J. Sotor, "Dissipative soliton generation in Er-doped fiber laser mode-locked by Sb_2Te_3 topological insulator," Opt. Lett. **40**, 2786 (2015).
195. J. Wang, J. Yin, T. He, and P. Yan, "Sb_2Te_3 mode-locked ultrafast fiber laser at 1.93 μm," Chin. Phys. B **27**, 084214 (2018).
196. J. Wang, Z. Jiang, H. Chen, J. Li, J. Yin, J. Wang, T. He, P. Yan, and S. Ruan, "High energy soliton pulse generation by a magnetron-sputtering-deposition-grown $MoTe_2$ saturable absorber," Photon. Res. **6**, 535 (2018).
197. J. Wang, Z. Jiang, H. Chen, J. Li, J. Yin, J. Wang, T. He, P. Yan, and S. Ruan, "Magnetron-sputtering deposited WTe_2 for an ultrafast thulium-doped fiber laser," Opt. Lett. **42**, 5010 (2017).
198. P. Yan, H. Chen, A. Liu, K. Li, S. Ruan, J. Ding, X. Qiu, and T. Guo, "Self-starting mode-locking by fiber-integrated WS_2 saturable absorber mirror," IEEE J. Quantum Electron. **23**, 33 (2017).
199. H. Chen, J. Yin, J. Yang, X. Zhang, M. Liu, Z. Jiang, J. Wang, Z. Sun, T. Guo, W. Liu, and P. Yan, "Transition-metal dichalcogenides heterostructure saturable absorbers for ultrafast photonics," Opt. Lett. **42**, 4279 (2017).
200. W. Liu, L. Pang, H. Han, W. Tian, H. Chen, M. Lei, P. Yan, and Z. Wei, "70-fs mode-locked erbium-doped fiber laser with topological insulator," Sci. Rep. **6**, 19997 (2016).
201. M. Kowalczyk, J. Bogusławski, R. Zybała, K. Mars, A. Mikuła, G. Soboń, and J. Sotor, "Sb_2Te_3-deposited D-shaped fiber as a saturable absorber for mode-locked Yb-doped fiber lasers," Opt. Mater. Express **6**, 2273 (2016).
202. P. Yan, Z. Jiang, H. Chen, J. Yin, J. Lai, J. Wang, T. He, and J. Yang, "α-In_2Se_3 wideband optical modulator for pulsed fiber lasers," Opt. Lett. **43**, 4417 (2018).
203. P. Yan, A. Liu, Y. Chen, H. Chen, S. Ruan, C. Guo, S. Chen, I. L. Li, H. Yang, J. Hu, and G. Cao, "Microfiber-based WS_2-film saturable absorber for ultrafast photonics," Opt. Mater. Express **5**, 479 (2015).
204. W. Liu, Y.-N. Zhu, M. Liu, B. Wen, S. Fang, H. Teng, M. Lei, L.-M. Liu, and Z. Wei, "Optical properties and applications for MoS_2-Sb_2Te_3-MoS_2 heterostructure materials," Photon. Res. **6**, 227 (2018).
205. Y. Meng, C. Zhu, Y. Li, X. Yuan, F. Xiu, Y. Shi, Y. Xu, and F. Wang, "Three-dimensional Dirac semimetal thin-film absorber for broadband pulse generation in the near-infrared," Opt. Lett. **43**, 1503 (2018).
206. J. Sotor, I. Pasternak, A. Krajewska, W. Strupinski, and G. Sobon, "Sub-90 fs a stretched-pulse mode-locked fiber laser based on a graphene saturable absorber," Opt. Express **23**, 27503 (2015).
207. G. Sobon, J. Sotor, I. Pasternak, A. Krajewska, W. Strupinski, and K. M. Abramski, "Thulium-doped all-fiber laser mode-locked by CVD-graphene/PMMA saturable absorber," Opt. Express **21**, 12797 (2013).
208. X. Wu, S. Yu, H. Yang, W. Li, X. Liu, and L. Tong, "Effective transfer of micron-size graphene to microfibers for photonic applications," Carbon **96**, 1114 (2016).
209. H. Xia, H. Li, C. Lan, C. Li, X. Zhang, S. Zhang, and Y. Liu, "Ultrafast erbium-doped fiber laser mode-locked by a CVD-grown molybdenum disulfide (MoS_2) saturable absorber," Opt. Express **22**, 17341 (2014).
210. P. Yan, H. Chen, J. Yin, Z. Xu, J. Li, Z. Jiang, W. Zhang, J. Wang, I. L. Li, Z. Sun, and S. Ruan, "Large-area tungsten disulfide for ultrafast photonics," Nanoscale **9**, 1871 (2017).
211. R. Khazaeizhad, S. H. Kassani, H. Jeong, D. Yeom, and K. Oh, "Passively mode-locked fiber laser based on CVD WS_2," in *CLEO* (2015), paper JW2A.74.
212. W. Liu, M. Liu, Y. O. Yang, H. Hou, M. Lei, and Z. Wei, "CVD-grown $MoSe_2$ with high modulation depth for ultrafast mode-locked erbium-doped fiber laser," Nanotechnology **29**, 394002 (2018).
213. W. Liu, M. Liu, J. Yin, H. Chen, W. Lu, S. Fang, H. Teng, M. Lei, P. Yan, and Z. Wei, "Tungsten diselenide for all-fiber lasers with the chemical vapor deposition method," Nanoscale **10**, 7971 (2018).

214. J. Wang, W. Lu, J. Li, H. Chen, Z. Jiang, J. Wang, W. Zhang, M. Zhang, I. L. Li, Z. Xu, W. Liu, and P. Yan, "Ultrafast thulium-doped fiber laser mode locked by monolayer WSe_2," IEEE J. Quantum Electron. **24**, 1100706 (2018).
215. J. Yin, J. Li, H. Chen, J. Wang, P. Yan, M. Liu, W. Liu, W. Lu, Z. Xu, W. Zhang, J. Wang, Z. Sun, and S. Ruan, "Large-area highly crystalline WSe_2 atomic layers for ultrafast pulsed lasers," Opt. Express **25**, 30020 (2017).
216. J. Wang, H. Chen, Z. Jiang, J. Yin, J. Wang, M. Zhang, T. He, J. Li, P. Yan, and S. Ruan, "Mode-locked thulium-doped fiber laser with chemical vapor deposited molybdenum ditelluride," Opt. Lett. **43**, 1998 (2018).
217. K. Zhang, M. Feng, Y. Ren, F. Liu, X. Chen, J. Yang, X.-Q. Yan, F. Song, and J. Tian, "*Q*-switched and mode-locked Er-doped fiber laser using $PtSe_2$ as a saturable absorber," Photon. Res. **6**, 893 (2018).
218. Q. Guo, J. Pan, Y. Liu, H. Si, Z. Lu, X. Han, J. Gao, Z. Zuo, H. Zhang, and S. Jiang, "Output energy enhancement in a mode-locked Er-doped fiber laser using CVD-Bi_2Se_3 as a saturable absorber," Opt. Express **27**, 24670 (2019).
219. G. Zhu, X. Zhu, F. Wang, S. Xu, Y. Li, X. Guo, K. Balakrishnan, R. A. Norwood, and N. Peyghambarian, "Graphene mode-locked fiber laser at 2.8 μm," IEEE Photon. Technol. Lett. **28**, 7 (2016).
220. K. Yin, T. Jiang, H. Yu, X. Zheng, X. Cheng, and J. Hou, "Mid-infrared ultrashort mode-locked fiber laser utilizing topological insulator Bi_2Te_3 nanosheets as the saturable absorber," arXiv:1505.06322 (2015).
221. Z. Qin, G. Xie, C. Zhao, S. Wen, P. Yuan, and L. Qian, "Mid-infrared mode-locked pulse generation with multilayer black phosphorus as saturable absorber," Opt. Lett. **41**, 56 (2015).
222. T. Hu, D. D. Hudson, and S. D. Jackson, "Stable, self-starting, passively mode-locked fiber ring laser of the 3 μm class," Opt. Lett. **39**, 2133 (2014).
223. Z. Qin, G. Xie, J. Ma, P. Yuan, and L. Qian, "2.8 μm all-fiber *Q*-switched and mode-locked lasers with black phosphorus", Photon. Res. **6**, 1074 (2018).
224. Z. Qin, T. Hai, G. Xie, J. Ma, P. Yuan, L. Qian, L. Li, L. Zhao, and D. Shen, "Black phosphorus *Q*-switched and mode-locked mid-infrared Er:ZBLAN fiber laser at 3.5 μm wavelength," Opt. Express **26**, 8224 (2018).
225. Z. Qin, G. Xie, H. Gu, T. Hai, P. Yuan, J. Ma, and L. Qian, "Mode-locked 2.8-μm fluoride fiber laser: from soliton to breathing pulse," Adv. Photon. **1**, 065001 (2019).
226. W. Du, H. Li, C. Lan, C. Li, J. Li, Z. Wang, and Y. Liu, "Graphene/WS_2 heterostructure saturable absorbers for ultrashort pulse generation in L-band passively mode-locked fiber lasers," Opt. Express **28**, 11514 (2020).
227. X. Hong, J. Kim, S.-F. Shi, Y. Zhang, C. Jin, Y. Sun, S. Tongay, J. Wu, Y. Zhang, and F. Wang, "Ultrafast charge transfer in atomically thin MoS_2/WS_2 heterostructures," Nat. Nanotech. **9**, 682 (2014).
228. Y. Yu, S. Hu, L. Su, L. Huang, Y. Liu, Z. Jin, A. A. Purezky, D. B. Geohegan, K. W. Kim, Y. Zhang, and L. Cao, "Equally efficient interlayer exciton relaxation and improved absorption in epitaxial and nonepitaxial MoS_2/WS_2 heterostructures," Nano Lett. **15**, 486 (2014).
229. K. S. Novoselov, A. Mishchenko, A. Carvalho, and A. H. Castro Neto, "2D materials and van der Waals heterostructures," Science **353**, aac9439 (2016).
230. J. Wang, Z. Li, H. Chen, G. Deng, and X. Niu, "Recent advances in 2D lateral heterostructures," Nano-Micro Lett. **11**, 48 (2019).
231. W. J. Liu, M. L. Liu, B. Liu, R. G. Quhe, M. Lei, S. B. Fang, H. Teng, and Z. Y. Wei, "Nonlinear optical properties of MoS_2-WS_2 heterostructure in fiber lasers," Opt. Express **27**, 6689 (2019).
232. Z. Wang, H. Mu, J. Yuan, C. Zhao, Q. Bao, and H. Zhang, "Graphene–Bi_2Te_3 heterostructure as saturable absorber for short pulse generation," ACS Photon. **9**, 832 (2015).
233. Y. Wang, H. Mu, X. Li, J. Yuan, J. Chen, S. Xiao, Q. Bao, Y. Gao, and J. He, "Observation of large nonlinear responses in a graphene-Bi_2Te_3 heterostructure at a telecommunication wavelength," Appl. Phys. Lett. **108**, 221901 (2016).
234. J. Wang, A. Coillet, O. Demichel, Z. Wang, D. Rego, A. Bouhelier, P. Grelu, and B. Cluzel, "Saturable plasmonic metasurfaces for laser mode locking," Light Sci. Appl. **9**, 50 (2020).
235. E. J. Lee, S. Y. Choi, H. Jeong, N. H. Park, W. Yim, M. H. Kim, J-K Park, S. Son, S. Bae, S. J. Kim, K. Lee, Y. H. Ahn, K. J. Ahn, B. H. Hong, J.-Y. Park, F. Rotermund, and D.-I. Yeom, "Active control of all-fibre graphene devices with electrical gating," Nat. Commun. **6**, 6861 (2015).
236. J. Bogusławski, Y. Wang, H. Xue, X. Yang, D. Mao, X. Gan, Z. Ren, J. Zhao, Q. Dai, G. Sobon, J. Sotor, and Z. Sun, "Graphene actively mode-locked lasers," Adv. Funct. Mater. **28**, 1801539 (2018).
237. K. Chen, X. Zhou, X. Cheng, R. Qiao, Y. Cheng, C. Liu, Y. Xie, W. Yu, F. Yao, Z. Sun, F. Wang, K. Liu, and Z. Liu, "Graphene photonic crystal fibre with strong and tunable light–matter interaction," Nat. Photon. **13**, 754 (2019).
238. S. Duval, M. Bernier, V. Fortin, J. Genest, M. Piché, and R. Vallée, "Femtosecond fiber lasers reach the mid-infrared," Optica **2**, 623 (2015).
239. T. Hu, S. D. Jackson, and D. D. Hudson, "Ultrafast pulses from a mid-infrared fiber laser," Opt. Lett. **40**, 4226 (2015).
240. C. Zhu, F. Wang, Y. Meng, X. Yuan, F. Xiu, H. Luo, Y. Wang, J. Li, X. Lv, L. He, Y. Xu, J. Liu, C. Zhang, Y. Shi, R. Zhang, and S. Zhu, "A robust and tuneable mid-infrared optical switch enabled by bulk Dirac fermions," Nat. Commun. **8**, 14111 (2017).